ResearchGate

See discussions, stats, and author profiles for this publication at: https://www.researchgate.net/publication/227697016

Predicted structures of agonist and antagonist bound complexes of adenosine A3 receptor

ARTICLE *in* PROTEINS STRUCTURE FUNCTION AND BIOINFORMATICS · JUNE 2011

Impact Factor: 2.63 · DOI: 10.1002/prot.23012

CITATIONS
10

READS
36

5 AUTHORS, INCLUDING:

Soo-Kyung Kim
California Institute of Technology
62 PUBLICATIONS **1,935** CITATIONS
SEE PROFILE

Lindsay Riley
University of California, Los Angeles
3 PUBLICATIONS **13** CITATIONS
SEE PROFILE

Kenneth A. Jacobson
National Institutes of Health
752 PUBLICATIONS **29,900** CITATIONS
SEE PROFILE

William A. Goddard
California Institute of Technology
1,322 PUBLICATIONS **66,663** CITATIONS
SEE PROFILE

Available from: Kenneth A. Jacobson
Retrieved on: 11 January 2016

PROTEINS
STRUCTURE ■ FUNCTION ■ BIOINFORMATICS

Predicted structures of agonist and antagonist bound complexes of adenosine A_3 receptor

Soo-Kyung Kim,[1] Lindsay Riley,[2] Ravinder Abrol,[1] Kenneth A. Jacobson,[3] and William A. Goddard III[1]*

[1] Division of Chemistry and Chemical Engineering, Materials and Process Simulation Center (MC139-74), California Institute of Technology, Pasadena, California 91125

[2] Department of Biomathematics, University of California, Los Angeles, California 90095

[3] Laboratory of Bioorganic Chemistry, Molecular Recognition Section, National Institute of Diabetes and Digestive and Kidney Diseases (NIDDK), National Institutes of Health (NIH), Bethesda, Maryland 20892

ABSTRACT

We used the GEnSeMBLE Monte Carlo method to predict ensemble of the 20 best packings (helix rotations and tilts) based on the neutral total energy (*E*) from a vast number (10 trillion) of potential packings for each of the four subtypes of the adenosine G protein-coupled receptors (GPCRs), which are involved in many cytoprotective functions. We then used the DarwinDock Monte Carlo methods to predict the binding pose for the human A_3 adenosine receptor (hAA_3R) for subtype selective agonists and antagonists. We found that all four A_3 agonists stabilize the 15th lowest conformation of apo-hAA_3R while also binding strongly to the 1st and 3rd. In contrast the four A_3 antagonists stabilize the 2nd or 3rd lowest conformation. These results show that different ligands can stabilize different GPCR conformations, which will likely affect function, complicating the design of functionally unique ligands. Interestingly all agonists lead to a *trans* χ1 angle for W6.48 that experiments on other GPCRs associate with G-protein activation while all 20 apo-AA_3R conformations have a W6.48 *gauche*+ χ1 angle associated experimentally with inactive GPCRs for other systems. Thus docking calculations have identified critical ligand-GPCR structures involved with activation. We found that the predicted binding site for selective agonist Cl-IB-MECA to the predicted structure of hAA_3R shows favorable interactions to three subtype variable residues, $I253^{6.58}$, $V169^{EL2}$, and $Q167^{EL2}$, while the predicted structure for $hAA_{2A}R$ shows weakened to the corresponding amino acids: $T256^{6.58}$, $E169^{EL2}$, and $L167^{EL2}$, explaining the observed subtype selectivity.

Proteins 2011; 79:1878–1897.
© 2011 Wiley-Liss, Inc.

Key words: docking; GPCR; agonists; antagonist; membrane protein predicted structure; adenosine receptor.

INTRODUCTION

Adenosine receptors (ARs), G protein-coupled receptors (GPCRs) with seven transmembrane (TM) spanning helices,[1] are involved in many cytoprotective functions, making them important pharmacological targets for treatment of a variety of diseases because of their key roles in controlling numerous physiological processes. Many therapeutic agents under development for treatment of central nervous system disorders, inflammatory diseases, asthma, kidney failure, and ischemic injuries exert their effects via direct interactions with ARs. However, the target is often just one of the four subtypes of human ARs, designated A_1, A_{2A}, A_{2B}, and A_3. The A_{2A} and A_{2B} adenosine subtypes are linked to Gs proteins, increasing the intracellular levels of cAMP upon receptor activation, while the A_1 and A_3 adenosine subtypes are linked to Gi proteins inhibiting cAMP formation. The A_3 and A_{2B} subtypes can also activate the inositol phosphate formation through coupling to Gq proteins.[2] Thus activation of human adenosine A_1 receptor (hAA_1R), decreases the oxygen demand of a stressed organ by slowing the heart rate. Conversely, activation of $hAA_{2A}R$ can increase oxygen supply via vasodilation and inhibition of platelet aggregation. Also a development of anti-Parkinson's agents utilizes $hAA_{2A}R$ antagonists.[3] On the other hand $hAA_{2B}R$ activation has an angiogenic effect, while activation of the cardiac hAA_3R preconditions cardiac myocytes against ischemic damage[4] and protects against toxicity.

Additional Supporting Information may be found in the online version of this article.
Abbreviations: AA_3R, adenosine A_3 receptor; GPCR, G protein-coupled receptor; vdW, van der Waals; TMH, transmembranic helix.

Grant sponsor: Gifts to the Materials and Process Simulation Center (MSC) (California Institute of Technology).
*Correspondence to: William A Goddard III, Materials and Process Simulation Center (MC139-74), California Institute of Technology, 1200 E. California Blvd., Pasadena, CA 91125. E-mail: wag@wag.caltech.edu.
Received 5 October 2010; Revised 20 January 2011; Accepted 1 February 2011
Published online 15 February 2011 in Wiley Online Library (wileyonlinelibrary.com).
DOI: 10.1002/prot.23012

© 2011 WILEY-LISS, INC.

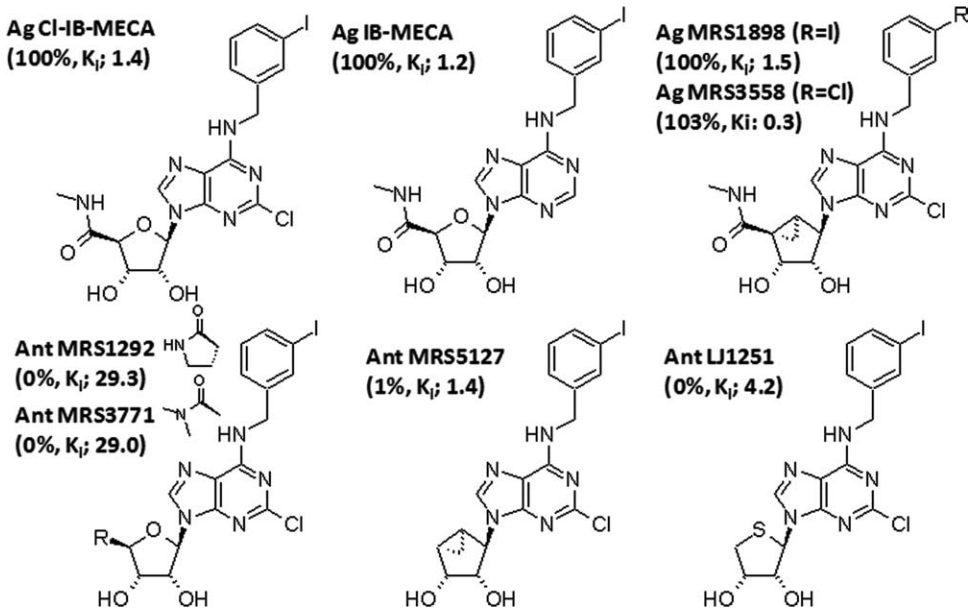

Chart 1

Structures of four agonists (Ag) and four antagonists (Ant) exhibiting selective binding to the adenosine A_3 receptor with respect to A_{2a}. Binding affinities (K_i in nM) are shown for A_3 with relative efficacies in parenthesis compared to the endogenous adenosine.

This can be seen in the case of the cardiotoxic effects of the anticancer drug doxorubicin.[5] Moreover, hAA_3R antagonists are of interest as potential antiglaucoma agents.[6] In particular, hAA_3R agonists, such as IB-MECA (N^6-(3-Iodobenzyl)-5′-*N*-methylcarboxamidoadenosine) and Cl-IB-MECA (2-Chloro-N^6-(3-iodobenzyl)-5′-*N*-methylcarboxamidoadenosine) that were developed in the Jacobson laboratory at National Institute of Health, are now advancing into Phase II clinical trials for treating diseases such as cancer, arthritis, and psoriasis.[2]

As these AR targets generally involve just one subtype, it is essential that new ligands be developed that are subtype specific. To design such subtype-selective drugs requires detailed 3D predicted structures for all four receptors and for the low-lying conformation that might be stabilized by the prospective new ligands. Particularly this is important for agonists, because it is likely that the process by which agonists activate the G-Protein involve the agonist interacting with more than one GPCR conformation.

Previously, we reported the predicted structures of the human adenosine subtypes (A_1, A_{2A}, A_{2B}, and A_3) based on the human β_2 adrenergic receptor template (PDB ID: 2rh1). There we found that the predicted binding energies of eight antagonists to the predicted structure of A_{2A} were found to correlate quite well with experiment. In addition the predicted binding sites for ZM241385 inverse agonist bound to $hAA_{2A}R$[7] compares well with x-ray crystal structure.

Here, we use the improved GEnSeMBLE method to predict new structures for the four subtypes (A_1, A_{2A}, A_{2B}, and A_3) of human AR starting with a template based on the x-ray structure for ZM241385 bound to $hAA_{2A}R$ (PDB ID: 3eml). GEnSeMBLE selects from a vast number (10 trillion) of potential packings a final ensemble of the 20 best packings (helix rotations and tilts) based on predicted total E, that we consider might play a role in binding to various ligands and in activation.

In addition, we used the DarwinDock Monte Carlo method to predict the binding sites and energies for four agonists and four antagonists (structures shown in Chart 1) to each of the 20 most stable conformations of hAA_3R. We find that all four agonists prefer the 15th conformation of the apo-hAA_3R, whereas the four antagonists prefer either the 2nd or 3rd. Moreover all four agonists have the W6.48 the horizontal orientation (*trans* χ_1) believed from experiments on other GPCRs to be associated with activation, while 20 lowest conformations of the apo-hAA_3R have W6.48 in the vertical orientation (*gauche*+ χ_1) believed from experiments on other GPCRs to be inactive.[8–10]

These predictions confirm the high selectivity toward hAA_3R for the agonist, Cl-IB-MECA, and the high selectively for adenosine toward $hAA_{2A}R$, the endogenous agonist, validating the accuracy of these methods for explaining the subtype selectivity.

We expect that improved understanding of how these GPCRs function at the molecular level will be useful for the development of novel classes of AA_3R-targeted drugs.

MATERIALS AND METHODS

To predict the 3D structures for the various conformations needed to understand the function of GPCRs and

help design new ligands, we use the GEnSeMBLE (GPCR Ensemble of Structures in Membrane BiLayer Environment) method, which provides a very complete sampling over possible rotations and tilts and leading to a ensemble of low lying predicted structures expected to include those conformations energetically accessible for binding of ligands. This replaces our earlier MembStruk method.[11]

We now use the DarwinDock to predict the binding sites of ligands to the GPCRs. This replaces our earlier HierDock[12] and MSCDock[13] methods, providing a much more complete sampling of possible poses. These earlier methods were validated by a series of applications to various GPCRs: human D_2 dopamine receptor (DR),[14] human β_2 adrenergic receptor,[15,16] human M_1 muscarinic receptor,[17] human Chemokine (C-C) motif receptor 1 (CCR1),[18] mouse MrgC11 (Mas Related Gene) for the molluscan peptide FMRF-amide (FMRFa),[19,20] human prostanoid DP receptor,[21] and human Serotonin 2C[22] receptor.

GEnSeMBLE consists of the following key steps:

Generation of the 7-transmembranic helix (TMH) bundle

PredicTM

To predict the seven TM domains our current approach (PredicTM) combines hydrophobicity analysis with information from multiple sequence alignments, involving six steps; (i) retrieval of similar protein sequences from a database, (ii) multiple sequence alignment of sequences using the MAFFT[23] program, (iii) Hydrophobic profile in the multiple sequence alignment (using the thermodynamic and biological hydrophobic scales from White and von Heijne[24,25]), (iv) initial TMH region predictions in Supporting Information Figure S1, (v) Application of capping rules and extension of consensus helices based on the APSSP2[26] and PORTER[27] servers, and (vi) identification of hydrophobic centers in Supporting Information Table S1. More details are described in Supporting Information.

OptHelix

To predict the kinks often induced by proline residues, we replace the longer side chains and helix termini (save Ser and Thr near Pro) with alanines and carry out 2 ns of molecular dynamics (MD) on each helix, followed by a restoration of the correct side chains using SCREAM[28] and a minimization of the structure. This procedure works well and predicts helices within 1-2 Å of the crystal.

Template generation

To pack the seven helices from OptHelix into a bundle requires that six quantities be specified for each helix: the x-, y-, and z-coordinate of the hydrophobic center, the tilt (θ) of each axis from the z-axis, the azimuthal orientation (ϕ) of this tilt; and the rotation (η) of the helix about the helical axis, when the x-axis is defined along the axis from the center point of TMH3 to the center point of TMH2 in the midplane (see Supporting Information Fig. S2). We obtain z from PredicTM while θ, ϕ, η are sampled as described later. The remaining two coordinates, x and y, for each helix are taken from template structures, either experimental or validated theoretical. Currently, we can consider eight such templates: bovRho (PDB ID: 1u19),[29] hβ_2-adrenergic receptor (2rh1),[10] hAA_{2A}R (3eml),[9] turkey β_1-adrenergic receptor (2vt4),[8] and bovine opsin (3cap)[30] from experiment, as well as the predicted and validated DP Prostaglandin,[21] MrgC11,[19,20] and CCR1 Chemokine[18] receptors. GEnSeMBLE allows for each of these templates to be used in separate predictions, providing an ensemble of bundles from which we can select on the basis of bundle *E* or ligand binding E.

As a reference for the rotation angle (η) of each helix, we use a highly conserved residue (N1.50, D2.50, W4.50, P5.50, P6.50, and P7.50) in family A and D3.32 that is conserved among amine receptors, and match the rotation angle of its Cα projection on the x-y plane to that of the corresponding residue in the template structure. The helical axis for rotation is defined as the one corresponding to the least moment of inertia axis obtained using all backbone atoms.

Homology of the 7-TMH bundle

HomologyTM

In addition to PredicTM helices, we also generated the homology TM helices where we took advantage of the high sequence identity of hAA_1R, hAA_{2B}R and hAA_3R with the x-ray structure of hAA_{2A}R, both at the whole sequence (A_1: 45.39%, A_{2B}: 38.59%, A_3:31.31%) and TMH region (A_1: 68.84%, A_{2B}: 59.94%, A_3: 51.01%) level. Using the sequence alignment of each subtype to hAA_{2A}R, the side chain of each amino acid in the isolated helices from the hAA_{2A}R bundle was mutated to the corresponding amino acid of the given subtype by our rotamer placement method SCREAM.[28]

For hAA_{2A}R, we constructed a TMH bundle from the x-ray structure, removing the N/C terminals and loops. The following residue number ranges describe the final TMH regions with α-helix structure: 5-32 for TMH1, 41-67 for TMH2, 75-106 for TMH3, 119-140 for TMH4, 175-204 for TMH5, 222-258 for TMH6, and 269-291 for TMH7.

OptimizeHelix

The geometry of each isolated helix was optimized by 100 steps with 0.5 terminal gradient using DREIDING 3 force field (FF) (referred to as DREIDING-III or D3FF)[31] to remove seriously bad contacts among helices.

BiHelix optimization of the rotation angles

BiHelix

The next step is to optimize the rotation angles (η) for each of the seven TMHs. The general procedure is to simultaneously rotate each TMH through 360° in 30° increments, leading to $(12)^7 = 35{,}000{,}000$ configures (Supporting Information Fig. S2). To rapidly identify the best 1000 of these, we first consider each helix interacting with just one other helix, leading to $12 \times 12 = 144$ combinations for each of the 12 pairs of interacting helices (1-2, 2-4, 4-5, 5-6, 6-7, 1-7, 1-3, 2-3, 3-4, 3-5, 3-6, 3-7). For each of these 144×12 pairs we optimize the sidechains using SCREAM.[28] Then these 1728 "mean field" numbers are used to estimate the energies of all 35,000,000 conformations, from which we pick the best 1000 by total *E* for subsequent CombiHelix analysis.

SCREAM uses a library of residue conformations ranging from a root mean square of a Cα atom (CRMS) diversity of 0.4 to 1.6 Å in conjunction with a Monte Carlo sampling using full valence, hydrogen bond and electrostatic interactions, but with special van der Waals (vdW) potentials that somewhat reduce the penalty for contacts that are slightly too short while retaining the normal attractive interactions at full strength. With SCREAM, we find that we can now base the selections on the total E, Escream, without separate considerations for valence, electrostatic, hydrogen bond, and vdW terms.

However for the ARs, we restricted rotations ±45° rotation with 15° increments resulting in $(7)^7 = 823{,}543$ combinations. Then we used the BiHelix to combine the Escream energies of the 49 combinations for each helix pair (using a total of 49×12 helix pairs = 551 energies) to estimate the *E* for all 823,543 conformational combinations for the ±45° rotational range.

CombiHelix

The top 1000 predicted structures from BiHelix analysis are built explicitly using the rotations specified for each helix in the combination. The multiple rotational combinations are minimized by their side chains using SCREAM to evaluate the total *E* of the optimized multihelix bundle. To avoid overestimation of long-range charge interaction, we neutralize the system by adding protons into the negatively charged residues, Asp and Glu, or by deleting protons from the positively charged amino acids, Lys and Arg. After neutralizing the top 100 predicted structures based on the charged total *E*, the final 100 low *E* predicted structures are ordered by the neutral total *E* of the optimized multi-helix bundle.

We validated this procedure for all five experimental GPCR structures. Using the BiHelix method, we estimated the energies for all $(12)^7 \sim 35$ million combinations from 0 to 360° angles by 30° increments. The experimental structure corresponds to the angle rotation combination 0_0_0_0_0_0_0 (the first zero corresponds to TMH 1, the second zero corresponds to TMH 2, and so on). The results indicate that the crystal structures rank as the top 1 lowest *E* predicted structure at the end of the procedure for all five cases.

SuperBiHelix optimization of the rotation and tilt angles

SuperBiHelix

For the lowest *E* predicted structures from BiHelix for each of the four subtypes, we determine the optimum rotations (θ, ϕ, η) for the packing of the seven helices into a 7-TMH bundle. Here we considered a ±10° sampling of θ tilt angle and a ±30° sampling of both ϕ and η angles, leading to a total of $(3 \times 5 \times 5)^7 \sim 10$ quadrillion combinations. To make this huge sampling computationally feasible, use SuperBiHelix sampling as follows. For each of the 12 pairs of helices, we sample all combinations of θ, ϕ, η for each of the $(3 \times 5 \times 5)^2 = 5625$ rotational-tilt combinations of each of the 12 pairs. In each case we optimize the side chains using SCREAM[28] with all-atom DREIDING FF.[31]

The total energies for each of these $(12) \times (5625)$ helix pair combinations are used to estimate the *E* for all 10 quadrillion 7-TMH bundle conformational combinations using the following procedure. To determine the conformations for each helix that lead to low *E* bundles. Then the 7-TMH bundle is partitioned into three quadhelix bundles. Next, the total energies of the three quadhelix bundles are calculated using the BiHelical energies. This is feasible because only $3 \times (3 \times 5 \times 5)^4 \approx 10^8$ bundle energies must be calculated. The 2000 predicted structures with the lowest *E* for each quadhelix are listed by increasing *E* and used to select the top 36 orientations preferred by each helix. Finally, these conformations are used to calculate the *E* of $(36)^7 \approx 8 \times 10^{10}$ full bundles and output the 1000 best *E* predicted structures from this procedure.

SuperComBiHelix

The top 2000 predicted structures from the SuperBiHelix analysis were built explicitly using the rotations and tilts specified for each helix in the combination (they will take different conformations than were found in the BiHelical mode). The seven TMH predicted structure is then minimized for 10 steps. This ensemble of low-lying predicted structures from SuperComBiHelix is used to in the docking studies for various agonists and antagonists.

The 100 lowest *E* predicted structures based on the charge total *E*, are then neutralized and reordered by the neutral total *E* of their optimized multihelix bundle. From this we select the ensemble of ~20 low-*E* predicted structures, each of which is docked to agonists, antagonists,

and inverse agonists to provide the structures likely to be involved in GPCR activation.

This procedure has been validated by applying it to all GPCRs.[7]

Our goal in developing these *in silico* methods is to predict the 3D structures of GPCRs that are remote from the systems currently available from experiment. Thus we have emphasized first principles approaches rather than homology methods. We believe that the studies reported in this article indicate the potential power of this approach. Thus we find that the ensemble of configurations of the apo-A_3 provides the flexibility to bind both to agonists and antagonists. As experimental methods are developed to obtained x-ray structures of agonist-bound systems, we will obtain quantitative measures for the accuracy of our predictions.

Ligand docking

The lowest *E* predicted structures of the $hAA_{2A}R$ and hAA_3R from BiHelix were used for docking several ligands, using the DarwinDock. The structure and charges of the ligands in Chart 1 were calculated using quantum mechanics (B3LYP with the 6-311G** basis set). The Histidines forming the H-bonding with Glu were treated as the protonated His with +1 charge. Those His are $H272^{7.43}$ in the hAA_3R and $H264^{EC3}$/$H278^{7.43}$in the $hAA_{2A}R$.

Scanning the receptor for potential binding regions

Starting with the predicted structure, we predicted putative ligands binding regions as follows. We first alanized the entire protein (replacing the 6 hydrophobic residues, I, L, V, F, Y, and W with A) and scanned for potential binding regions with no assumption about the binding site. The entire molecular surface of the predicted structure was mapped with spheres representing the empty volume of the protein (currently using the Sphgen procedure in DOCK4.0 suite of programs). The entire set of protein spheres is partitioned into ~30 to 50 overlapping cubes of 10 to 14 Å sides. We then generated 1000 poses for each of these 30–50 regions. These results are compared to select the most promising two or three putative binding regions.

DarwinDock

Our earlier studies used the HierDock and GenMSCDock, which have now been replaced by DarwinDock. For each ligand conformation, DarwinDock iteratively generates ~50,000 poses into the putative binding regions of the bulky-residue-alanized protein. This is followed by the *E* scoring of family heads to select the top 10% ordered by total *E*. The top 100 conformations are chosen for further optimization. For each of these we dealanize the protein side-chains (using SCREAM) to find the optimum side chains for each of the best 100 poses. Then we neutralize the protein and ligand by transferring protons appropriately within salt bridges and protonating or deprotonating exterior ligands, followed by further full geometry minimization.

This same procedure was followed for each of seven ligand conformations generated as follows. Starting from the x-ray structure of adenosine crystal, we rotated the torsion angles C_{ar}-C_{ar}-NH-C_{al} and C_{ar}-NH-C_{al}-C_{ar} between the adenine ring and the benzyl substituent by 60° increments to generate 36 conformations. These were generated with the Maestro software and minimized with the D3FF. We selected the lowest seven ligand conformations (within 3 kcal/mol of the best E) for docking in Supporting Information Table S2 as described earlier. The final docked structure with the best binding *E* from all ligand conformations was selected.

DarwinDock has been validated for a number of x-ray cocrystals including three crystal structures of ligand/GPCR complexes: human β_2-adrenergic receptor (0.4 Å RMSD),[10] human $AA_{2A}R$ (0.8 Å RMSD),[9] and turkey β_1-adrenergic receptor (0.1 Å RMSD).[8] This shows that we can accurately identify ligand binding sites in proteins, which can then be used to optimize the ligands with desirable properties.

Neutralization for scoring E

Quantum mechanics (QM) calculations show that for an effective dielectric constant is <8Å, the extra proton on a Lys or Arg transfers back to the negative carboxylate of an Asp or Glu.[22] Thus we expect that buried salt bridges will have neutral residues. We consider that use of these neutral residue charges improves the accuracy for comparing different docked structures. Of course the final bond energy relative to ligand in the solvent and binding site exposed to solvent must be corrected by the effective pK of the bare Lys, Arg, Glu, Asp or of the ligand, a correction that is simple to make. For example, if the pK of a carboxylate is 4.5 and the solvent is taken to have a pH of 7.4 we must correct by 2.9 × 1.38 kcal/mol.

For external residues not involved in binding, we find it expedient to neutralize the external residues exposed to solvent or membrane. Here the issue is that the force fields commonly used in MD calculations involve fixed charges, usually based on QM. In reality any net partial charges are shielded by the dielectric polarization of the surrounding protein and solvent so that there is negligible effect by 10Å. However with fixed charges the electrostatic interaction energy between two point charges separated by 10Å is 33 kcal/mol. The result is that small changes in geometries of charged ligands far from the binding site can lead to large differential binding energies, even 10 to 30 kcal/mol. We find that neutralizing these exposed residues removes the sensitivity to details of the distances of charged residues (and counter ions) remote from the active site. This neutralization leads to differential binding energies that

are dominated by the local cavity interactions and leads to much smaller solvation energies.

MD studies

To validate the stability of the Monte Carlo structures predicted herein, each ligand-protein predicted structure was inserted into a fully equilibrated hydrated POPC lipid bilayer having cell size in the XY plane of 75 Å × 75 Å (172 POPC molecules) and solvated with 6689 water molecules using Membrane builder in the VMD program. This was done for predicted structure **1** of the LJ1251 antagonist bound to predicted structure **2** and the Cl-IB-MECA agonist bound to predicted structure 15 with the disulfide bridge between 88 and 166. The procedure here was identical to that in Kim *et al.*[32]

The lipid tails were almost fully extended, allowing for easy insertion of the protein into the membrane. The distance between the layers was set at $c = 72.3$ Å to fit the actual membrane thickness plus the solvent thickness. The lateral supercell was set to fit the actual surface density of lipid molecules, $a = 69.9$ and $b = 68.4$ Å. We introduced disorder into the lipid bilayer patches to better resemble a membrane at 300K by allowing random orientation of each lipid about its axis with a short (1ps) equilibration at 300K in vacuum. This eliminated steric contacts between the lipid atoms but left the lipid tails mostly extended. These steps in our procedure reduce the time required for equilibration of the lipid/protein complex. After inserting the protein into the lipid-water cell, lipids overlapping within 1 Å of protein and waters overlapping within 5 Å were removed.

For the particle mesh Ewald (PME) in the electrostatics calculation,[33] the charge of system was balanced through replacing waters into 13 Cl^- ions. These systems contain 37,661 atoms (A_3 selective agonist Cl-IB-MECA-hAA_3R), and 367,645 atoms (A_3 selective antagonist LJ1251-hAA_3R). This predicted structure was then equilibrated at 300K for 1 ns using the NAMD 2.5 (NAnoscale Molecular Dynamics) program.[34] We used the CHARMM22 force field parameters for the protein, the TIP3 model for water,[35] and the CHARMM27 force field parameters for the lipids.[36] Minimization of both ligands in vacuum for these ligands led to bond lengths, angles, and dihedrals similar to the quantum mechanical results and the previous predicted structures determined with DREIDING.[31] Quantum charges from DFT/6311G** method were used for these ligands.

RESULTS AND DISCUSSIONS

GEnSeMBLE predictions of the ensemble of low lying conformations of all four ARs

As summarized in Methods, the GEnSeMBLE method for predicting 3D structures of GPCRs aims at sampling a complete set of helix conformation with the emphasis on the rotations of the helices about their axis and on the tilts of these helices and then selecting the top ~20 based on energetic. We start with a template to define the six degrees of freedom for each helix (x, y, z, θ, ϕ, η) for each of the 7 helices and first consider all possible rotation angles (η) about the helix axes. Generally GEnSeMBLE allows each η angle to go over 360°, in increments of 30°, leading to $(7)^{12} = 35{,}000{,}000$ different combinations. However, for the ARs, we considered each η angle from −45° to +45° in 15° increments leading to $(7)^7 = 823{,}000$ combinations. This is because an x-ray structure was available for hAA_{2A}R and the similarity of the four subtypes from the multiple sequence alignment in Figure 1 suggests that the rotational angles would change by less than 45°. Supporting this, the analysis of relative differences of the six degrees of freedom for each helix (x, y, z, θ, ϕ, η) among the x-ray structures of GPCRs, β_1 and β_2 adrenergic receptor between two subtypes differs less than ±10° in the rotational (η) angle of each helix, as shown in Supporting Information Table S3. Indeed despite the major differences between hAA_{2A}R and human β_2 adrenergic receptor, the variation of the rotational (η) angle of each helix is within ±20°. In addition, the comparison of bovine rhodopsin to opsin (which is believed to be an equilibrium active state structure) suggests a range of ±30° in rotational angle variations (Supporting Information Table S4). Thus, our sampling angle of ±45° can generate the ground-state structure as well as the active state structure.

As described in Methods, we used the BiHelix mean field strategy to rapidly estimate the energies of the 823,000 packings, selecting the lowest E 1000 to build into full 7-TMH bundles with optimum side chains (CombiHelix). The top 10 predicted structures of hAA_{2A}R and hAA_3R ranked by neutral total E are shown in Table 1. The other top 10 predicted structures of hAA_1R and hAA_{2B}R are displayed in Supporting Information Table S5. We find that the best packing predicted structure for hAA_{2A}R has exactly the same rotation angles as the experimental hAA_{2A}R (denoted as the all-0° predicted structure).

The same procedure was used for all four subtypes, but except for hAA_3R, all ARs prefer the same $\eta = 0°$ angles as hAA_{2A}R.

For hAA_{2A}R, we find that the top 10 predicted structures have variations of ± 15° for TMHs 1 and 4 and +15° for TMHs 3, 5, and 6.

For hAA_1R we find that the top 10 predicted structures have variations of +15° for TMHs 3 and 7, ± 15° for TMH5, +15/ +45° for TMH6, and ± 15/ +30° for TMH4.

For hAA_{2B}R we find helix rotation preferences similar to hAA_{2A}R (reasonable based on the sequence identity of ~60% in the TMH region between these two ARs), with rotational variations of +15° for TMHs 4 and 6, ± 15° for TMH5, and −15° for TMH1.

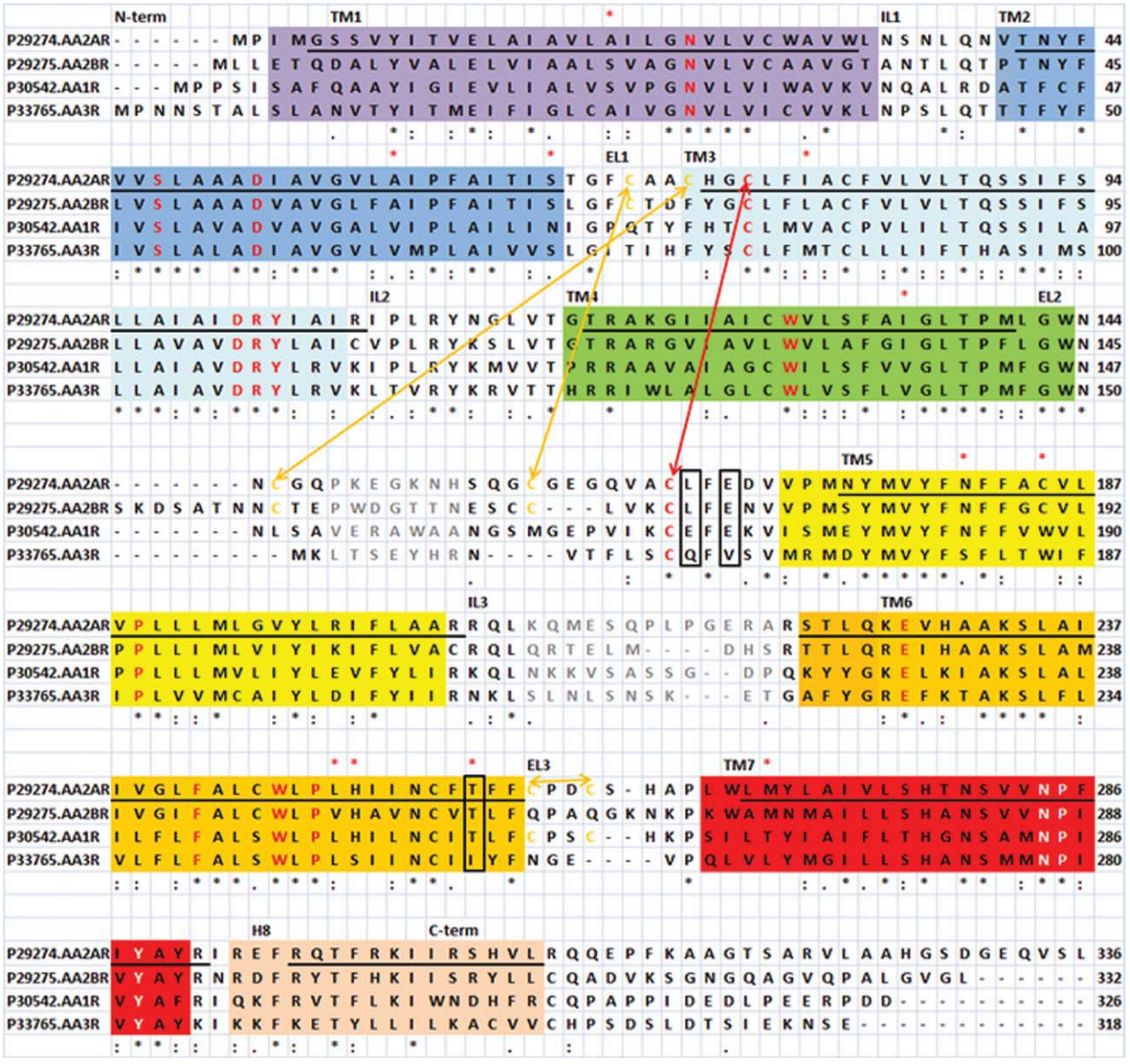

Figure 1

Alignments of the four adenosine receptor (AR) subtypes, A_1, A_{2A}, A_{2B}, and A_3 from the PredicTM method. The predicted TMH regions from PredicTM are displayed in colored boxes (TMH1 in purple, TMH2 in blue, TMH3 in cyan, TMH4 in green, TMH5 in yellow, TMH6 in orange, TMH7 in red), while the TMH region from the x-ray structure of the $AA_{2A}R$ (PDB: 3eml) is underlined. Highly conserved residues in Family A G protein-coupled receptors (GPCRs) are shown in red in TMH 1-6 and white in TMH7. Variable amino acids among the four subtypes in the upper TMH regions are marked with red asterisks and subtype selective residues predicted from the cavity analysis are boxed. The disulfide bridges in yellow were assigned (A_1: 80-169, 260-263, A_{2A}: 71-159, 74-146, 77-166, 259-262, A_{2B}: 72-167, 78-171, A_3: 83-166) based on the sequence alignment. We use Ballesteros-Weinstein numbering consisting of the TMH helix number followed by residue number relative to the highly conserved residue in the helix, numbered as 50. H-bonding is indicated by arrows, and subtype selective residues are shown in red.

For hAA_3R, the lowest E predicted structure has TMH4-rotated by $+15^\circ$. The top 10 predicted structures show rotational variations of -15° for TMHs 2 and 7, $+15^\circ$ for TMH3, $\pm$ 15° for TMH4, and $+15$, $+30^\circ$ for TMH6.

After determining the range of optimum η angles for the top 10 conformations of the four subtypes, we then optimized the θ (tilt) and ϕ (sweep) angles. Here we started with the η's of the best conformation and varied η and ϕ over the range of -30, -15, 0, 15, 30° while sampling θ for -10, 0, 10°. This leads to $(75)^7 = \sim 13$ trillion (13,348,388,671,875) combinations. To make it practical to estimate the energies of all these packings, we used the SuperBiHelix mean field strategy described in

Table I
Top 10 Predicted Structures of Human Adenosine A_{2A} and A_3 Receptors from the CombiHelix Analysis of the $(7)^7$ = 823,000 BiHelix Packing Geometries Within ±45° Angle Range by 15° Increments

H1	H2	H3	H4	H5	H6	H7	ChargeIH	ChargeTot	NeutIH	NeuTot	W6.48 χ1
A_{2A}											
0	0	0	0	0	0	0	−379.3	158.8	−397.8	13.7	−79.5
0	0	0	15	0	0	0	−356.2	169.7	−380.3	14.2	−79.5
0	0	0	−15	0	0	0	−380.2	189.7	−399.6	47.0	−79.5
−15	0	0	0	0	0	0	−364.6	216.9	−382.1	60.2	−79.5
−15	0	0	15	0	0	0	−347.3	220.3	−369.5	60.2	−79.5
0	0	0	0	15	0	0	−328.1	245.6	−350.2	84.2	−79.2
0	0	0	0	15	15	0	−325.0	250.0	−344.8	90.7	−145.0
0	0	15	0	0	0	0	−354.4	254.8	−383.4	93.1	−79.5
15	0	0	15	0	0	0	−323.1	262.1	−344.9	93.2	−79.5
0	0	0	15	15	15	0	−311.9	248.2	−330.6	93.8	−81.0
A_3											
0	0	0	15	0	0	0	−354.9	430.3	−327.6	292.5	174.9
0	0	0	0	0	0	0	−359.2	418.7	−341.5	299.6	−79.1
0	0	15	15	0	15	0	−347.5	421.1	−331.4	309.4	−174.5
0	0	0	0	0	30	−15	−347.7	443.1	−337.0	311.5	163.9
0	0	0	15	0	15	0	−381.0	445.4	−356.0	315.3	−179.6
0	−15	15	15	0	15	0	−339.0	414.1	−308.2	319.5	−179.7
0	0	0	0	15	15	0	−325.0	464.4	−320.7	321.5	−179.5
0	0	0	−15	0	0	0	−354.5	442.7	−317.5	322.7	−79.1
0	0	15	−15	0	15	0	−368.9	421.6	−322.7	324.0	−174.6
0	0	0	15	15	15	0	−318.4	479.0	−313.2	324.8	153.4

All 1000 predicted structures from CombiHelix were selected for neutralization by their charge total energy score (ChargeTot: kcal/mol). The final 100 predicted structures are ordered by neutral total energy (NeutTot: kcal/mol). The case with η = 0 ° for all 7 helices (same as in the experimental antagonist bound A_{2A}R structure) is shown in gray shading. Thus there is a change only for AA_3R in TMH4 by +15°. ChargeIH (Charge interhelical energy), ChargeTot (Charge total energy), NeutIH (Neutral interhelical energy), NeutTot (Neutral total energy)

the methods sections. Here we select the best 2000 conformations to build into full 7-TMH bundles with optimum side chains, selecting the best based on *E* for subsequent docking. These results for hAA_3R are shown in Table 2 where the all 0° predicted structure corresponds to the best predicted structure from CombiBiHelix, which had TMH4 rotated 15°. Among the top 20 predicted structures for hAA_3R we find

η variations of −15° for TMHs 1 and 4

θ differences of −10° for TMH4 and +10° for TMH5.

ϕ changes of ± 15° for TMHs 4 and 7, 15° for TMH5, and ± 15, −30° for TMH6.

Thus there are favorable variations at TMHs 4, 5, 6, 7 within +15°. The various salt-bridges and the H-bonding networks of the predicted structure in the D(E)RY and NPxxY region are summarized in Supporting Information Table S6. Among these top 20 predicted structures, we find an average of 10 inter-helical hydrogen bonds (HB). A_3 has a specific H-bonding network among $Y109^{3.51}$, $K113^{3.55}$ and $D199^{5.60}$. These interactions are not observed in the x-ray structure of $hAA_{2A}R$, because the amino acid corresponding to $D190^{5.60}$ in hAA_3R is Arg in $hAA_{2A}R$.

The 15th predicted structure of apo-A_3 that is best for binding of selective agonists shows a weakened interaction of TMHs 1-2-7 H-bonding networks among $N30^{1.50}$, $D58^{2.50}$, and $N278^{7.49}$, as shown in Supporting Information Table S6. The H-bonding distances of $N30^{1.50}$: $N278^{7.49}$ and $D58^{2.50}$: $N278^{7.49}$ are 4.6 and 4.9 Å, respectively, while the corresponding H-bond distances in the 1st and 2nd model are 2.9 and 2.7 Å, respectively. However the salt-bridge and the H-bonding in the D(E)RY region ($D107^{3.49}$: $R111^{3.53}$, $D107^{3.49}$: $R126^{4.41}$, $R108^{3.50}$: $E225^{6.30}$, $E225^{6.30}$: $R224^{6.29}$ $K113^{3.55}$: $D199^{5.60}$, $Y109^{3.51}$: $K113^{3.55}$) are similar among them.

We show below that several of these best 20 predicted structures might play a role in differential binding of agonists, antagonists, and inverse agonists, as well as in activation pathways.

Ensemble docking of hAA_3R selective agonists

We then docked the hAA_3R selective agonists and selective antagonists in Chart 1 to each of the best 20 predicted structures in Table 2 from SuperBiHelix.

We found variations in the orientation and packing of several of the TMH (especially TMHs 4, 5, 6, 7) in the top 20 predicted structures as follows: tilting +10° for TMHs 4 and 5, sweeping angles of ± 15° for TMHs 4/ 5 and ± 15, -30° for TMHs 6/ 7, and rotation of −15° for TMHs 1/ 4.

As shown in Table 3 and Figure 2, we find that all four agonists,

- Cl-IB-MECA,
- IB-MECA,
- MRS1898 ((1's, 2′*R*, 3's, 4′*R*, 5's)-4-{2-Iodo-6-[(3-iodophenylmethyl)amino]-purine-9-yl}-1-(methylaminocarbonyl)bicycle-[3.1.0]-hexame-2,3-diol), and

Table II
Top 20 Predicted Structures of Human A_3 Adenosine Receptor From the SuperBiHelix/CombiHelix Analysis Using the Range (−10, 0, 10°) for θ (Tilting) and the Range (−30, −15, 0, 15, 30°) for ϕ (Sweep) and η (Rotation) Angles

	θ (°)							ϕ (°)							η (°)							
Ser. No.	H1	H2	H3	H4	H5	H6	H7	H1	H2	H3	H4	H5	H6	H7	H1	H2	H3	H4	H5	H6	H7	NeutTot
1	0	0	0	0	0	0	0	0	0	0	0	0	0	0	0	0	0	0	0	0	0	147.4
2	0	0	0	0	0	0	0	0	0	0	0	0	15	0	0	0	0	−15	0	0	0	155.1
3	0	0	0	0	10	0	0	0	0	0	15	0	−30	0	0	0	0	−15	0	0	0	158.8
4	0	0	0	0	0	0	0	0	0	0	0	0	0	−15	0	0	0	−15	0	0	0	164.4
5	0	0	0	0	10	0	0	0	0	0	0	0	−30	0	0	0	0	−15	0	0	0	166.0
6	0	0	0	0	10	0	0	0	0	0	15	0	−15	0	0	0	0	−15	0	0	0	170.6
7	0	0	0	0	10	0	0	0	0	0	0	0	−30	0	0	0	0	0	0	0	0	171.4
8	0	0	0	0	0	0	0	0	0	0	0	0	15	15	0	0	0	0	0	0	0	172.6
9	0	0	0	0	0	0	0	0	0	0	0	0	15	−15	0	0	0	−15	0	0	0	174.2
10	0	0	0	0	10	0	0	0	0	0	15	0	−30	0	0	0	0	0	0	0	0	174.4
11	0	0	0	0	10	0	0	0	0	0	0	0	−15	0	0	0	0	−15	0	0	0	176.8
12	0	0	0	0	0	0	0	0	0	0	0	0	15	15	0	0	0	−15	0	0	0	177.8
13	0	0	0	0	10	0	0	0	0	0	15	0	−30	−15	0	0	0	−15	0	0	0	182.4
14	0	0	0	0	10	0	0	0	0	0	0	15	−30	0	0	0	0	−15	0	0	0	183.2
15	0	0	0	0	0	0	0	0	0	0	−15	0	15	0	0	0	0	−15	0	0	0	183.3
16	0	0	0	0	10	0	0	0	0	0	0	0	−15	0	−15	0	0	−15	0	0	0	183.8
17	0	0	0	0	10	0	0	0	0	0	15	0	−30	−15	0	0	0	0	0	0	0	184.7
18	0	0	0	0	10	0	0	0	0	0	15	0	−30	−30	0	0	0	0	0	0	0	185.0
19	0	0	0	−10	10	0	0	0	0	0	−15	0	−30	0	0	0	0	−15	0	0	0	186.6
20	0	0	0	0	10	0	0	0	0	0	0	0	−15	−30	0	0	0	−15	0	0	0	187.3

All 1000 predicted structures from CombiHelix by charge total energy (ChargeTot: kcal/mol), were selected for neutralization and the final 100 predicted structures were ordered by neutral total energy (NeutTot: kcal/mol). The case with η = 0° for all seven helices is shown in gray shading. This corresponds to the 0, 0, 0, 15, 0, 0, 0° lowest NeutTot energy predicted structure from Bihelix in Table 1. Supporting Information Table S1 includes detailed analysis of the salt-bridge and the H-bonding networks among top 20 predicted structures. All cases have the *gauche*+ χ1 angle for W243$^{6.48}$, the rotamer trigger angle associated with the inactive state.

- MRS3558 ((1's, 2′*R*, 3's, 4′*R*, 5's)-4-{2-Chloro-6-[(3-iodophenylmethyl)amino]-purine-9-yl}-1-(methylaminocarbonyl)bicycle-[3.1.0]-hexame-2,3-diol),
  Prefer to bind to the 15th lowest conformation from SuperBiHelix (TMH4 ϕ: −15°, TMH6 ϕ: 15°, TMH4 η: −15°).

Ensemble docking of hAA$_3$R selective antagonist

On the other hand three antagonists,

- MRS3771 [(2*S*,3*S*,4*R*,5*R*)-5-[2-Chloro-6-(3-iodo-benzylamino)-purin-9-yl]-3,4-dihydroxy-tetrahydrofuran-2-carboxylic acid dimethylamide],
- LJ1251 [(2*R*, 3*R*, 4*S*)-2-(2-Chloro-6-(3-iodobenzylamino)-9*H*-purin-9-yl)tetrahydrothiophene-3,4-diol] and
- MRS1292 [(2*R*, 3*R*, 4*S*, 5*S*)-2-[N^6-3-Iodobenzyl]adenos-9′-yl]-7-aza-1-oxa-6-oxospiro[4.4]-nonan-4,5-diol],
  Prefer to bind to the predicted structure 2 from Table 3 (TMH6 ϕ: 15°, TMH4 η: -15°).
- Whereas antagonist
- MRS5127 [(1′*R*, 2′*R*, 3's, 4′*R*, 5's)-4′-[2-chloro-6-(3-iodobenylamino)-purine]-2′, 3′-*O*-dihydroxybicyclo-[3.1.0]-hexane],
  Prefers predicted structure 3 with TMH4 ϕ: 15°, TMH6 ϕ: -30°, TMH4 η: -15°. The second best predicted structure for MRS5127 is also predicted structure 2 of Table 1.

This exception of MRS5127 might arise from a different signaling system. MRS5127 was highly AA_3R-selective (Binding affinity at three human AR subtypes: hA_1 = 3040 ± 610 nM, hA_{2A} = 1080 ± 310 nM, hA_3 = 1.44 ± 0.6 nM). By Schild analysis of [^{35}S]GTPγS binding to membranes from CHO (Chinese Hamster Overlay) cells expressing the hAA_3R, MRS5127 appeared to be an antagonist.[37] However, further analysis determined that it is a partial agonist stimulating cAMP (cyclic adenosine monophosphate) production in transfected cells with 45% efficacy compared to the full agonist NECA (Adenosine 5′-*N*-ethyluronamide).[38]

LJ1251 acts more uniformly as an antagonist both in GTPγS binding and in cyclase experiments, but MRS5127 leads to differences in the functional assay.

Comparison of conformations for binding agonists and antagonists

The 20 most stable predicted structures for the apo protein all have a *gauche*+ χ_1 rotamer preference for W6.48 (leading to the vertical orientation with respect to the membrane plane) that has been implicated from experiments on other GPCRs to be associated with the inactive form.[8–10]

Table III
SuperCombiHelix Top 20 Predicted Structures for the Human Adenosine A_3 Receptor, Including Agonists (left) and Antagonists (right), Ordered by Neutral Total Energy Including Solvation (TotSol Energy) (kcal/mol)

Agonist						Antagonist					
CIIBMECA	Tot	UCav	ComSol	TotSol	W243χ1	MRS1292	Tot	UCav	ComSol	TotSol	W243χ1
15-A3	−79.8	−19.3	−267.1	−346.9	**154**	2-A3	−67.9	−22.4	−268.1	−336.0	**177**
3-A3	−81.5	−23.4	−257.8	−339.4	*−71*	15-A3	−64.1	−23.0	−268.2	−332.3	**177**
2-A3	−63.3	−20.7	−266.1	−329.4	**−165**	1-A3	−55.2	−15.5	−273.1	−328.3	*−87*
1-A3	−56.9	−20.5	−271.7	−328.6	**−175**	12-A3	−68.2	−21.2	−256.3	−324.5	*−87*
5-A3	−65.8	−18.6	−261.1	−326.8	*−69*	9-A3	−57.1	−15.9	−261.6	−318.8	*−85*
12-A3	−71.3	−24.3	−255.5	−326.8	**−164**	3-A3	−56.1	−19.0	−256.8	−312.8	*−119*
9-A3	−59.7	−18.8	−260.2	−319.9	**155**	4-A3	−32.8	−17.5	−274.6	−307.3	*−87*
4-A3	−46.9	−18.7	−272.2	−319.1	**−175**	8-A3	−49.2	−18.0	−254.8	−304.0	*−87*
8-A3	−58.9	−23.0	−255.0	−313.8	**−164**	13-A3	−30.0	−14.4	−269.1	−299.1	**178**
6-A3	−49.6	−25.4	−263.6	−313.2	**−171**	5-A3	−37.2	−18.7	−260.6	−297.8	*−119*
13-A3	−41.3	−13.1	−266.0	−307.3	*−69*	19-A3	−27.7	−19.5	−255.0	−282.6	**177**
11-A3	−34.8	−17.0	−268.6	−303.4	**−171**	11-A3	−10.5	−16.1	−267.0	−277.6	*−119*
19-A3	−45.5	−13.9	−252.8	−298.4	*−69*	16-A3	−24.9	−17.4	−251.3	−276.2	*−119*
7-A3	−35.3	−20.8	−262.2	−297.5	*−71*	6-A3	−13.4	−17.7	−262.5	−275.9	*−118*
16-A3	−41.1	−22.1	−252.4	−293.5	**−171**	7-A3	−10.3	−19.1	−261.3	−271.6	*−119*
10-A3	−30.8	−22.7	−261.7	−292.6	*−71*	14-A3	−3.2	−16.6	−267.1	−270.3	*−119*
20-A3	−21.2	−19.4	−268.8	−290.0	**−171**	18-A3	1.1	−10.2	−268.2	−267.1	**177**
14-A3	−18.8	−17.5	−267.9	−286.7	**−166**	17-A3	0.4	−12.9	−264.6	−264.2	**177**
18-A3	−18.7	−11.4	−267.3	−286.0	*−69*	10-A3	−3.9	−18.3	−260.2	−264.1	*−118*
17-A3	−13.9	−17.7	−261.9	−275.8	*−69*	20-A3	3.8	−18.9	−267.2	−263.4	**−171**

IBMECA	Tot	UCav	ComSol	TotSol	W243χ1	MRS3771	Tot	UCav	ComSol	TotSol	W243χ1
15-A3	−75.6	−19.7	−267.1	−342.6	**155**	2-A3	−80.9	−26.5	−267.9	−348.8	**−165**
1-A3	−62.8	−20.5	−271.5	−334.3	**−175**	15-A3	−69.0	−26.1	−268.6	−337.6	**−166**
3-A3	−75.3	−21.9	−257.4	−332.8	*−71*	9-A3	−66.8	−26.9	−260.7	−327.5	**155**
2-A3	−59.1	−20.0	−266.2	−325.3	**−165**	12-A3	−63.2	−26.8	−255.8	−318.9	**−164**
12-A3	−69.1	−23.1	−255.8	−325.0	**−164**	1-A3	−42.8	−24.2	−271.7	−314.5	**−175**
5-A3	−60.1	−18.1	−261.1	−321.2	*−69*	4-A3	−39.1	−23.2	−274.9	−314.1	**−175**
9-A3	−54.9	−18.4	−260.1	−315.0	**155**	3-A3	−54.5	−28.9	−255.9	−310.4	*−79*
4-A3	−43.1	−17.9	−271.8	−314.9	**−175**	8-A3	−48.7	−26.1	−254.3	−303.0	**−165**
8-A3	−56.8	−22.1	−254.5	−311.3	**−164**	16-A3	−49.0	−24.5	−251.4	−300.4	**−171**
13-A3	−36.2	−12.1	−265.6	−301.8	*−70*	13-A3	−26.2	−21.8	−266.5	−292.7	**−166**
6-A3	−36.7	−23.6	−263.4	−300.1	**−171**	11-A3	−22.3	−22.1	−267.7	−290.0	**−171**
11-A3	−30.7	−16.1	−269.0	−299.7	**−171**	5-A3	−29.7	−25.8	−259.4	−289.1	*−82*
19-A3	−39.5	−13.3	−253.5	−292.9	*−69*	6-A3	−13.2	−26.8	−261.9	−275.1	**−164**
14-A3	−23.4	−19.1	−267.4	−290.8	**−166**	7-A3	−10.5	−27.3	−260.0	−270.5	*−79*
7-A3	−28.3	−19.6	−261.8	−290.1	*−71*	19-A3	−17.9	−24.4	−251.7	−269.6	*−82*
16-A3	−36.9	−21.2	−251.6	−288.5	**−171**	14-A3	−1.0	−22.7	−265.7	−266.7	**−167**
20-A3	−19.6	−19.8	−268.3	−287.9	**−171**	10-A3	−3.1	−28.3	−259.2	−262.3	*−79*
10-A3	−24.4	−21.1	−260.9	−285.3	*−71*	17-A3	4.7	−20.9	−261.2	−256.5	**−166**
18-A3	−14.7	−12.6	−266.0	−280.7	*−69*	20-A3	8.6	−24.3	−262.8	−254.1	**−166**
17-A3	−7.5	−16.6	−260.9	−268.4	*−69*	18-A3	14.6	−25.3	−265.3	−250.7	*−81*

MRS1898	Tot	UCav	ComSol	TotSol	W243χ1	MRS5127	Tot	UCav	ComSol	TotSol	W243χ1
15-A3	69.7	−17.8	−267.5	−197.8	**154**	3-A3	49.2	−17.0	−260.2	−211.0	*−79*
3-A3	66.4	−17.0	−260.7	−194.2	*−71*	2-A3	56.4	−16.9	−265.7	−209.3	*−80*
1-A3	80.9	−12.8	−274.9	−193.9	*−70*	1-A3	67.8	−13.6	−273.9	−206.1	*−80*
2-A3	79.2	−20.1	−265.7	−186.5	**−165**	15-A3	69.6	−15.6	−266.5	−197.0	*−80*
5-A3	77.5	−17.3	−263.2	−185.8	*−70*	12-A3	63.7	−16.6	−255.5	−191.8	*−79*
9-A3	82.1	−18.7	−259.9	−177.8	**154**	9-A3	71.5	−14.6	−260.7	−189.2	*−86*
4-A3	96.9	−12.2	−273.5	−176.6	*−70*	4-A3	89.9	−11.3	−−274.5	−184.6	*−81*
12-A3	80.4	−20.7	−255.5	−175.1	**−164**	5-A3	79.3	−15.6	−262.1	v182.8	*−81*
13-A3	103.5	−12.7	−268.6	−165.1	*−70*	6-A3	92.0	−19.7	−265.5	−173.5	*−80*
8-A3	94.2	−19.0	−256.1	−161.9	**−164**	19-A3	83.2	−15.7	−254.7	−171.5	*−81*
6-A3	106.3	−18.9	−264.3	−158.0	*−71*	13-A3	97.7	−11.7	−268.6	−170.9	*−81*
11-A3	112.3	−17.8	−267.5	−155.2	*−70*	8-A3	85.3	−14.9	−255.3	−170.1	*−79*
7-A3	114.1	−15.6	−264.8	−150.7	*−72*	11-A3	99.4	−16.5	−268.5	−169.0	*−81*
19-A3	103.8	−17.4	−253.4	−149.6	*−70*	14-A3	108.0	−16.0	−267.8	−159.8	*−80*

(Continued)

Table III
(Continued)

MRS1898	Tot	UCav	ComSol	TotSol	W243χ1	MRS5127	Tot	UCav	ComSol	TotSol	W243χ1
16-A3	105.4	−17.8	−254.0	−148.6	*−72*	16-A3	95.3	−20.1	−253.8	−158.5	*−80*
10-A3	118.4	−16.2	−264.9	−146.6	*−71*	10-A3	107.7	−16.4	−264.3	−156.6	*−79*
18-A3	125.1	−7.3	−269.5	−144.4	*−70*	7-A3	112.7	−16.1	−264.0	−151.3	*−79*
14-A3	127.9	−20.2	−267.8	−140.0	**−166**	20-A3	125.1	−6.8	−265.9	−140.8	*−96*
20-A3	131.6	−5.7	−265.4	−133.8	*−70*	17-A3	126.9	−10.9	−264.2	−137.2	*−81*
17-A3	135.0	−11.4	−264.0	−129.0	*−70*	18-A3	135.3	−4.4	−269.5	−134.3	*−96*

−MRS3558	Tot	UCav	ComSol	TotSol	W243χ1	LJ1251	Tot	UCav	ComSol	TotSol	W243χ1
15-A3	69.2	−18.5	−265.6	−196.4	**154**	2-A3	−88.6	−17.5	−265.6	−354.3	*−80*
1-A3	79.6	−13.5	−273.1	−193.5	*−70*	1-A3	−78.0	−20.3	−273.1	−351.1	*−80*
3-A3	68.6	−17.3	−259.2	−190.6	*−71*	12-A3	−92.4	−17.3	−256.2	−348.6	*−79*
2-A3	77.7	−19.9	−265.6	−187.9	**−165**	15-A3	−80.7	−18.0	−266.6	−347.3	*−80*
5-A3	79.7	−18.1	−262.1	−182.4	*−70*	3-A3	−90.4	−19.3	−256.8	−347.2	*−79*
9-A3	81.4	−20.0	−259.2	−177.8	**155**	4-A3	−54.4	−11.6	−273.8	−328.2	*−80*
4-A3	94.4	−12.4	−272.2	−177.8	*−70*	9-A3	−68.4	−10.2	−259.8	−328.1	*-85*
12-A3	79.3	−21.5	−254.7	−175.5	**−164**	5-A3	−59.2	−18.0	−259.6	−318.7	*−80*
13-A3	105.9	−10.6	−267.1	−161.2	*−70*	8-A3	−63.4	−20.6	−255.0	−318.5	*−79*
8-A3	93.4	−20.4	−253.9	−160.5	**−164**	16-A3	−57.5	−18.9	−251.8	−309.2	*−79*
16-A3	98.8	−16.3	−253.3	−154.5	*−72*	6-A3	−43.6	−19.5	−263.0	−306.6	*−80*
6-A3	108.2	−15.0	−262.4	−154.2	*−71*	14-A3	−39.3	−13.6	−266.9	−306.2	*−80*
10-A3	112.4	−17.0	−262.6	−150.2	*−71*	19-A3	−53.1	−19.1	−252.3	−305.4	*−80*
7-A3	116.2	−14.2	−263.6	−147.4	*−71*	11-A3	−37.8	−17.5	−266.1	−303.9	*−81*
19-A3	106.1	−16.3	−252.5	−146.4	*−70*	13-A3	−34.5	−18.4	−265.9	−300.3	*−81*
11-A3	121.2	−16.5	−266.4	−145.2	*−70*	10-A3	−32.0	−18.7	−260.6	−292.6	*−79*
18-A3	132.3	−8.4	−267.1	−134.8	*−70*	7-A3	−28.4	−19.5	−260.8	−289.2	*−79*
20-A3	129.4	−9.1	−263.6	−134.2	*−70*	18-A3	−14.6	−16.8	−266.9	−281.5	*−96*
14-A3	131.7	−18.7	−265.1	−133.4	**−166**	20-A3	−14.8	−15.1	−264.5	−279.3	*−96*
17-A3	137.2	−9.3	−261.7	−124.5	*−69*	17-A3	−15.1	−16.7	−262.1	−277.2	*−81*

The lowest energy predicted structure is shown in gray shading. Although we consider TotSol Energy to be the most accurate for ranking the predicted structures, we have included three other energies also useful in ranking ligand-bound proteins: Tot, UCav, and ComSol. The lowest state predicted by these measures are indicated with an underline. The χ1 angle of W243$^{6.48}$ is shown at the right for each case. From studies on other GPCRs, this angle of W6.48 is considered to serve as a rotamer trigger switch for activation of the G-protein, with *gauche+* corresponding to the inactive state and *trans* corresponding to the active state. Here we put the cases with trans (active) in bold face, with the *gauche+* cases (inactive) in italics. The predicted ground state for all four agonists have the *trans* (active form), while all 20 lowest strucrures for the apo-hAA$_3$R have the *gauche+* (inactive form). For the antagonist systems, two 5′-truncated antagonists (LJ1251 and MRS5127) have the *gauche* (inactive form) for the all 20 lowest conformations, while the other two have a *trans* (active state) but many low lying *gauche* (inactive) excited configuraions.

We predicted the bound structure of the agonist (Cl-IB-MECA) to each of these predicted 20 lowest apo-hAA$_3$R structures and found that the predicted best structure (to apo-15) and 60% of the 20 show a preference of W6.48 for the *trans* χ1 rotamer (leading to the horizontal orientation with respect to the membrane plane). Previous experiments on other GPCRs have indicated that the *trans* χ_1 rotamer W6.48 is involved in activation.[39,40]

These results indicate that the mere binding the agonist to the apo-hAA$_3$R structure already can reposition the W6.48 conformation from the inactive form to the active form. This may prepare the agonist bound protein for a step that leads to activation, and hence it could be involved in activation as suggested by experiments on other GPCRs.[39,40]

Previous experiments on other GPCRs have also suggested that Y7.53 and R3.50 might also serve as rotamer switch upon activation.[41] However, considering each of the top 20 predicted apo-hAA$_3$R structures bound to either agonists or antagonists, Supporting Information Table S7, shows that the χ_1 angles of Y282$^{7.53}$ and R108$^{3.50}$ in the ligand-bound predicted structures have values nearly identical to the apo-protein. Thus the χ_1 angle of Y282$^{7.53}$ is -65° in apo- and antagonist-hAA$_3$R and -68° for agonist-hAA$_3$R. Similarly the χ_1 angle of R108$^{3.50}$ is -74° in apo-hAA$_3$R, -73° in antagonist-hAA$_3$R and -73° for agonist-hAA$_3$R. This can be compared to the χ_1 angles of are -74.31 for Y282$^{7.53}$ and -81.43° for R108$^{3.50}$ in opsin (PDB ID: 3cap). It may be that the Y7.53 and R3.50 residues play a later step in activation not sampled by our ensemble of structures and dynamics or it may be that hAA$_3$R does not involve these toggling events.

Supporting Information Figure S3 compares the best predicted structure for agonist Cl-IB-MECA/hAA$_3$R to the opsin crystal structure. Here we see similar values for the orientation of the three toggle switch residues, W243$^{6.48}$, Y282$^{7.53}$, and R108$^{3.50}$. This would suggest that in our apo protein structures, Y282$^{7.53}$ and R108$^{3.50}$ are already in their active form.

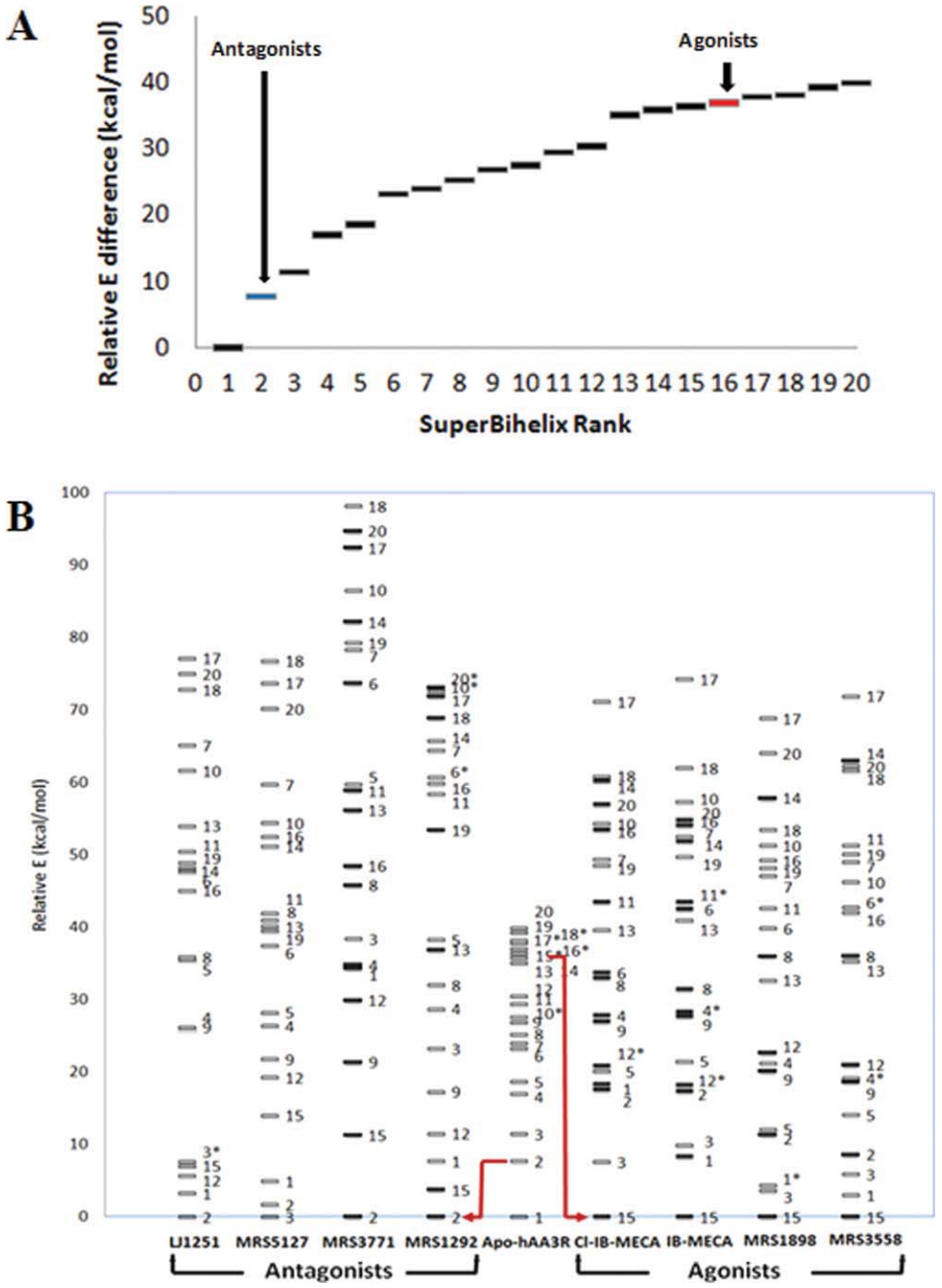

Figure 2

Graphical summary of ensemble docking in Table 3. The relative energies for apo and antagonist or agonist-bound human adenosine A_3 receptors (hAA_3R) are displayed. We find that all four A_3 selective agonists stabilize the 15th lowest conformation of hAA_3R while also binding strongly to the 1st and 3rd. In contrast three antagonists stabilize the 2nd lowest conformation of hAA_3R while antagonist MRS5127 prefers the 3rd but binding to the 2nd is next best. Experimentally the function of MRS5127 is ambiguous. It appeared to be an antagonist but acted as a partial agonist in cAMP (cyclic Adenosine monophosphate) production in transfected cells with 45% efficacy compared to the full agonist NECA (Adenosine 5′-*N*-ethyluronamide). All 20 lowest predicted structures for the apo hAA_3R have the "toggle switch" W6.48 in the *gauche*+ $\chi 1$ ($NH\text{-}C_\alpha\text{-}C_\beta\text{-}C_\gamma$) rotamer (tryptophan plane perpendicular to the membrane plane) associated with the inactive G protein-coupled receptor (GPCR) while the lowest predicted structures for the agonist bound state all have the *trans* $\chi 1$ ($NH\text{-}C_\alpha\text{-}C_\beta\text{-}C_\gamma$) rotamer (tryptophan plane parallel to the membrane plane) associated with the active GPCR. The situation is more ambiguous for the antagonist cases. Here MRS5127 and LJ1251 retain *gauche*. The cases with this *trans* rotamer are denoted by filled boxes while the cases with the *gauche*+ rotamer have open boxes. For cases in which the boxes overlap, the higher energy one was shifted higher to avoid overlapping. These cases are marked with asterisks. [Color figure can be viewed in the online issue, which is available at wileyonlinelibrary.com.]

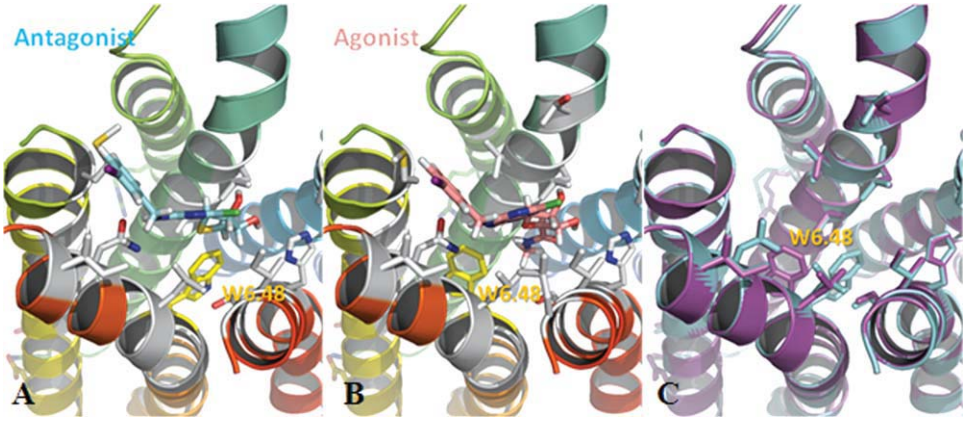

Figure 3

Predicted best structures of selective nucleoside antagonist LJ1251 bound to adenosine A_3 receptor (AA_3R) (**A**), selective agonist Cl-IB-MECA bound to adenosine A_3 receptor (AA_3R) (**B**) and superimposition of antagonist (blue)/agonist (red) bound predicted structures (**C**) without ligands. We predicted the binding to the top 20 predicted structures from the SuperBihelix analysis of the apo-AA_3R as shown in Table 3. LJ1251 binds to predicted structure 2 of apo-AA_3R while Cl-IB-MECA binds to predicted structure 15 of apo-AA_3R The orientation of the W6.48 side chain, shown in yellow, in the agonist-bound hAA_3R is perpendicular to the AA_3R axis and toward TMH5, while its orientation in the antagonist binding parallel to the AA_3R axis allowing it to interacts with the NPxxY motif, just as in the best predicted structure of the apo-AA_3R.

Supporting Information Table S7 shows that for apo-hAA_3R the top 20 predicted structures from SuperBihelix all have the *gauche*+ $\chi1$ rotamers of W6.48.

Table 3 shows that the best conformation (#15 of apo-hAA_3R) for all four agonists has the *trans* $\chi1$ conformation of W6.48. Indeed, this conformation is found in 12 of the top 20 in the Cl-IB-MECA and IB-MECA-hAA_3Rs and in 6 of the top 20 for the MRS1898 and MRS350-hAA_3Rs.

Similarly Table 3 shows that the 5′-truncated antagonists, MRS5127 and LJ1251, docked to hAA_3R all show *gauche*+ $\chi1$ rotamers of W6.48 (conformation 2). In contrast the 5′-modifed MRS3771 and MRS1292 prefer the *trans* $\chi1$ conformation.

Figure 3 shows the predicted structure 15 of agonist Cl-IB-MECA and the predicted structure 2 of the antagonist LJ1251 which features strongest interactions with the ligand molecule from DarwinDock (Table 3). The orientation of the W6.48 side chain in the agonist-bound hAA_3R is toward TMH5, while the W6.48 in the antagonist bound hAA_3R, is the same as in the apo-protein, which interacts with the NPxxY motif. That is, the agonists all induce a rotamer switch of W6.48 during upon binding. Indeed we find that the agonist-bound predicted structures are highly unfavorable in the *gauche*+ $\chi1$ conformation of W6.48. Thus Figure 4 shows how the total cavity *E* depends on a *trans* versus *gauche*+ $\chi1$ rotamer of W6.48. All agonist-bound complexes lead to an increase in the *E* of $> \sim$12 kcal/mol in the *gauche*+ $\chi1$ form of W6.48 due to steric bumps with 5′-substituents.

In contrast, we find the antagonist-bound predicted structures lead to similar cavity energies for both conformations. For nucleoside antagonists containing 5′-substituents (MRS1292 with 5′-cyclized uronamide and MRS3771 with 5′-*N*,*N*-dimethyl uronamide) are $\sim$3 kcal/mol unfavorable in the *gauche*+ $\chi1$ form of W6.48. However, MRS5127 and LJ1251, which are truncated at the 5′-position, are more stable in the *gauche*+ $\chi1$ conformation of W6.48.

The predicted rotamer switch of $W243^{6.48}$ induced by binding of the agonist found in this study is consistent with some experimental observations.[42] Thus the W243A mutation in hAA_3R dramatically impaired functional coupling but did not diminish agonist affinity. Also W243F affected function but did not diminish agonist affinity. Thus we conclude that binding the agonist induces reorientation of the $W243^{6.48}$ side chain which affects the receptor's transition from an inactive to an active state.

We find specific interactions of the ribose moiety in its hydrophilic pocket at T3.36, S7.42, and H7.43. This complex is stabilized by inward movement of F5.43 and the characteristic outward rotation of W6.48 as found in previous docking studies.[43]

Several previous studies on various GPCRs have suggested that W6.48 functions as a rotamer toggle switch from inactive *gauche*+ to active *trans*. The available experimental 3D structures of GPCRs bound to an inverse agonist or antagonist[8–10,29] all have W6.48 constrained in the inactive *gauche*+ conformation either by a network of interactions through water (bRho and the β_1, β_2

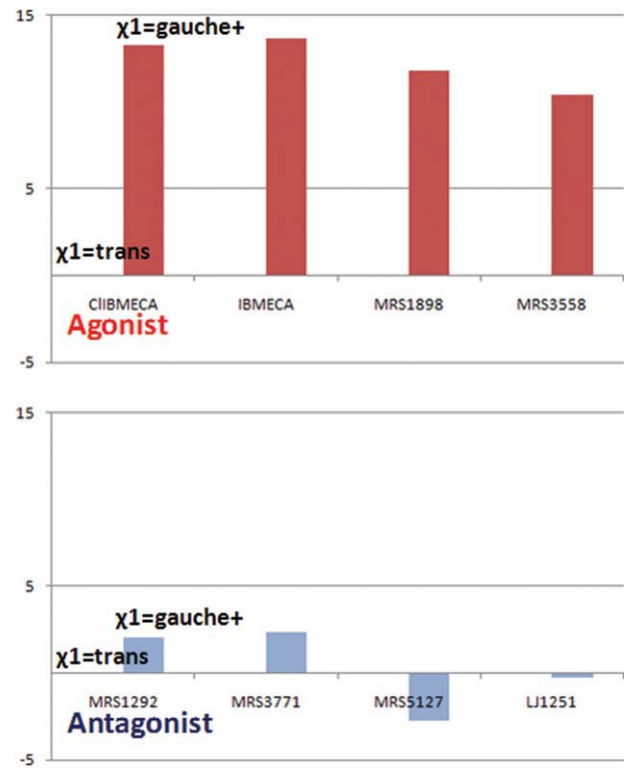

Figure 4

The relative difference of total cavity energy depending on the *trans* versus *gauche*+ χ1 (NH-C_α-C_β-C_γ) rotamer states of W6.48. All top agonist-bound complexes have over ~12 kcal/mol higher *E* in the *gauche*+ χ1 form of W6.48 because of steric bumps with 5′-substituents. However, all antagonist-bound predicted structures have similar energies for both conformations. In the case of nucleoside antagonists with 5′-substituents, the 5′-cyclized uronamide in MRS1292 and 5′-*N*,*N*-dimethyl uronamide in MRS3771 are < ~3 kcal/mol unfavorable in the *gauche*+ χ1 form of W6.48. However, MRS5127 and LJ1251, which were truncated at the 5′-position, are more stable in the *gauche*+ χ1 conformation of W6.48. [Color figure can be viewed in the online issue, which is available at wileyonlinelibrary.com.]

adrenergic receptors) or by an extension of N7.45 ($hAA_{2A}R$) to D2.50. The x-ray structure of metarhodopsin I suggests that W6.48 undergoes a conformational transition during the process of receptor activation, where it shifts from pointing toward TMH7 in the inactive *gauche*+ conformation to pointing toward TMH5 in the active *trans* conformation.[39] Based on the Conformational Memories biased Monte Carlo technique it was concluded that rotamer changes of C/S/T6.47, W6.48, and F6.52 in β_2 adrenergic receptor are highly correlated, representing a rotamer "toggle switch" that may modulate the TMH6 Pro-kink.[44]

On the other hand site-directed mutagenesis and molecular modeling approaches suggest that the 5-hydroxytryptamine-4 receptor involves different side-chain conformational toggle switches, that is, T3.36 from inactive *gauche*- to active *gauche*+ and W6.48 from inactive *gauche*+ to active *trans*.[40]

MD on ligand-protein in membrane and solvent

The above predictions represented the presence of the membrane and water using implicit solvation methods. To test the effect of explicit interactions with membrane and solvent, we inserted each ligand-protein predicted structure into a fully equilibrated hydrated palmitoyl-oleyl-phosphatidylcholine (POPC) lipid bilayer and water, which was subsequently equilibrated for 10 nanoseconds. All charged residues (Asp, Glu, Lys, and Arg) were treated as charged amino acids with CHARMM22 force field parameters.[35]

The potential *E* (Supporting Information Fig. S4) shows reasonable convergence in 10 ns, suggesting that the predicted structures are reasonably close to a local minimum.

In particular for the agonists the MD finds that the 15th lowest predicted structure (average RMSD of protein and ligand: 1.5 and 1.3 Å) remains more stable than the first predicted structure (average RMSD of protein and ligand: 2.3 and 2.6 Å), while for the antagonist the second predicted structure (average RMSD of protein and ligand: 2.1 and 1.9 Å) remains more stable than the first predicted structure (average RMSD of protein and ligand: 2.6 and 2.1 Å).

Our predicted structures lead to no significant changes in the salt-bridges or polar contacts for these cases. However, for the agonist Cl-IB-MECA/ hAA_3R complex, we found increased stability of the salt-bridge between $D107^{3.49}$ and $R126^{4.41}$ compared with LJ1251/ hAA_3R complex. The predicted salt bridge from $R108^{3.50}$ of the D(E)RY motif of TMH3 with $E225^{6.30}$ of TMH6 remains intact during these dynamics (Supporting Information Fig. S5).

As shown in Figure 5, the W6.48 rotamer for both agonist and antagonist retains the same conformation (horizontal for agonist vs. vertical for antagonist) during the dynamics. We found no significant changes in the salt-bridges or polar contacts for these cases in the predicted structures.

These limited MD studies validate the local stability of the predicted structures. However, we anticipate that it will take much longer dynamics (perhaps 1–1000 μs) to observe the changes involved with activation.

Subtype selectivity through docking studies using the DarwinDock method

As summarized in Methods the DarwinDock method for predicting ligand binding sites, starts by sampling the full protein to locate putative binding regions, and then aims at sampling a complete set of ligand conformation for each of which we sample a complete set of poses, from which we use the total binding *E* to select the best poses.

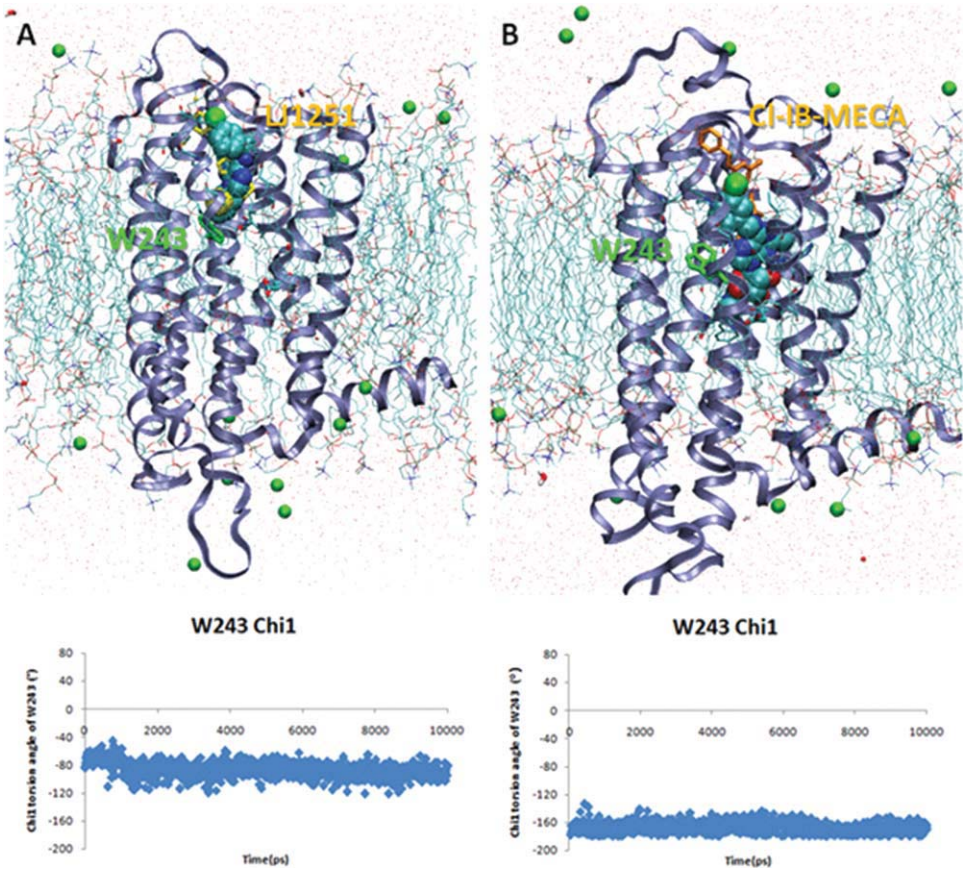

Figure 5

Molecular dynamics simulation of (**A**) antagonist LJ1251 in yellow and (**B**) agonist Cl-IB-MECA in orange bound human adenosine A_3 receptor (hAA_3R) in explicit lipid and water. Bottom) $\chi 1$ torsion angle (NH-C_α-C_β-C_γ) variation of $W243^{6.48}$ in green through 10 ns simulations. Ligand at the beginning is represented by the stick model and ligand at 10ns is shown in vdW (van der Waals) drawing mode of the visual molecular dynamics (VMD) program.

$hAA_{2A}R$ selective adenosine

Since adenosine has ~30-fold higher selectivity to $hAA_{2A}R$ than hAA_3R, we docked adenosine, the endogenous agonist, to the lowest *E* predicted structure of $hAA_{2A}R$ of Table 1. Supporting Information Table S8 lists the final 25 poses out of the 5000 conformations generated by DarwinDock.

All poses show similar ribose packing, and indeed nearly all adenosine agonists maintain similar ribose moieties, except for the amide substitution at the 5′-position. Indeed an intact furanose moiety is present in most potent adenosine agonists previously developed.[45] Our cavity analysis (see Table 4) of the adenosine bound to $hAA_{2A}R$ shows that the three major contributing amino acids are $N253^{6.55}$ (−7.22 kcal/mol), $F168^{EL2}$ (−6.33 kcal/mol), and $E169^{EL2}$ (−5.13 kcal/mol), based on nonbonding energies (defined in the methods section as the sum of vdW, electrostatic Coulomb with 2.5 dielectric constant and H-bond energies).

In the predicted structure of adenosine-$hAA_{2A}R$, we find that the exo-cyclic amino group of the adenine ring interacts with $N253^{6.55}$ and $E169^{EL2}$ in the same way that it interacts with the amino group in the tri-cyclic ring of ZM241385 seen in the x-ray structure of $hAA_{2A}R$, as shown in Figures 6A and 7A. An additional predicted interaction (−2.82 kcal/mol) occurs between the 2′ and 3′—OH group of the nucleoside ring and the side chains of the double protonated basic $H278^{7.43}$, which also interacts with $E13^{1.39}$. Supporting this, the Ala mutation of $N253^{6.55}$ shows loss of agonist and antagonist binding, while the $H278E^{7.43}$ mutation displays substantial decrease of agonist and antagonist binding except in the case of N^6-substituted agonists.[46]

We then matched the predicted ligand binding structure from $hAA_{2A}R$ to hAA_3R, leading to common interactions at $N250^{6.55}$ (−5.82 kcal/mol), $F168^{EL2}$ (−4.52 kcal/mol), and $H272^{7.43}$ (−4.03 kcal/mol). However, $V169^{EL2}$ in hAA_3R corresponds with $E169^{EL2}$ in $hAA_{2A}R$ losing the interaction with the terminal amino group,

Table IV
Cavity Energy of the Endogenous Agonist Adenosine Bound to the Human Adenosine A_3 (AA_3R) and A_{2A} Receptors ($AA_{2A}R$)

$AA_{2A}R$ Ki: estimated 30 nM						AA_3R Ki: estimated 1000 nM					
Res	#	VdW	Coulomb	H-Bond	NonBond	Res	#	VdW	Coulomb	H-Bond	NonBond
ASN	253	3.86	−3.03	−8.05	−7.22	ASN	250	2.41	−2.64	−5.59	−5.82
PHE	168	−6.49	0.16	0.00	−6.33	PHE	168	−4.57	0.05	0.00	−4.52
GLU	**169**	**−0.42**	**−1.16**	**−3.55**	**−5.13**	**VAL**	**169**	**0.00**	**0.00**	**0.00**	**0.00**
HSE	278	−1.02	−0.08	−1.72	−2.82	HSE	272	0.20	−0.68	−3.55	−4.03
ILE	274	−2.82	0.10	0.00	−2.72	ILE	268	−2.25	0.23	0.00	−2.02
VAL	**84**	**−2.14**	**−0.24**	**0.00**	**−2.39**	**LEU**	**90**	**1.37**	**−0.30**	**0.00**	**1.07**
LEU	249	−2.15	−0.04	0.00	−2.19	LEU	246	−3.31	−0.07	0.00	−3.39
SER	277	−0.45	0.08	−1.41	−1.78	SER	271	−1.28	−0.49	0.00	−1.77
LEU	85	−1.39	−0.10	0.00	−1.49	LEU	91	−0.88	−0.08	0.00	−0.96
MET	177	−1.35	−0.04	0.00	−1.39	MET	177	−1.29	−0.05	0.00	−1.34
THR	88	−0.56	−0.63	−0.11	−1.29	THR	94	−0.38	−0.42	0.00	−0.80
MET	**270**	**−1.05**	**0.00**	**0.00**	**−1.05**	**LEU**	**264**	**−1.28**	**0.01**	**0.00**	**−1.27**
ALA	63	−0.44	−0.05	0.00	−0.49	ALA	69	−0.33	−0.04	0.00	−0.37
HIS	**250**	**−0.41**	**0.11**	**0.00**	**−0.30**	**SER**	**247**	**0.00**	**0.00**	**0.00**	**0.00**
ILE	**66**	**−0.26**	**0.01**	**0.00**	**−0.25**	**VAL**	**72**	**−0.19**	**0.01**	**0.00**	**−0.18**
ALA	**81**	**−0.30**	**0.06**	**0.00**	**−0.24**	**THR**	**87**	**−0.73**	**0.06**	**0.00**	**−0.67**
ILE	252	−0.21	0.04	0.00	−0.17	ILE	249	−0.19	0.07	0.00	−0.12
MET	174	−0.20	0.03	0.00	−0.17	MET	174	0.00	0.00	0.00	0.00
GLU	13	−0.09	−0.06	0.00	−0.15	GLU	19	0.00	0.00	0.00	0.00
TRP	246	0.00	0.00	0.00	0.00	TRP	243	−1.92	−0.01	0.00	−1.94
LEU	**167**	**0.00**	**0.00**	**0.00**	**0.00**	**GLN**	**167**	**−0.31**	**−0.13**	**0.00**	**−0.44**
ALA	**59**	**0.00**	**0.00**	**0.00**	**0.00**	**VAL**	**65**	**−0.33**	**−0.01**	**0.00**	**−0.34**
THR	**256**	**0.00**	**0.00**	**0.00**	**0.00**	**ILE**	**253**	**−0.12**	**0.08**	**0.00**	**−0.04**
SUM					**−37.56**	**SUM**					**−28.92**

Residues are ordered by total NonBond energy (A_{2A}), which is the sum of van der Waals (vdW), Coulomb, and H-bond energy (kcal/mol) in the unified cavity. Subtype residues that are predicted to vary between A_{2A} and A_3 are displayed in bold face. The main interactions leading to subtype selectivity (underlined) in the predicted structure are E169 in A_{2A} vs. V169 in A_3, and V84 in A_{2A} vs. L90 in A_3. The color coding for contributions of each residue to binding of the adenosine ligand is: Dark gray: > 3 kcal/mol, Gray: 1–3 kcal/mol, Light gray: 0.5–1.0 kcal/mol.

resulting in unfavorable interactions in hAA_3R because of the different loop geometry of EL2 (Table 4 and Fig. 7B). The result is a dramatic decrease in binding affinity (cavity sum = −37.56 for $hAA_{2A}R$ vs. −28.92 for hAA_3R) in agreement with the dramatically decreased experimental binding affinity of endogenous adenosine at both rat ARs ($rAA_{2A}R$ estimated K_i: 30 nM vs. rAA_3R estimated K_i, 1000 nM).[45]

hAA_3R selective Cl-IB-MECA agonist

We docked Cl-IB-MECA to the lowest *E* predicted structure of hAA_3R of Table 1. From DarwinDock we selected the final 125 poses (five different ligand conformations with 25 poses each) out of 25,000 conformations. These predicted structures were ordered by the average rank of neutral total and Unified cavity *E* (UniCav E) in Supporting Information Table S9. From the cavity analysis of A_3 subtype selective Cl-IB-MECA bound to hAA_3R, Table 5 shows that the major contributing amino acids are $F168^{EL2}$ (−9.79 kcal/mol), $N250^{6.55}$ (−4.44 kcal/mol), $L246^{6.51}$ (−4.28 kcal/mol), and $H272^{7.43}$ (−3.35 kcal/mol). The terminal benzyl group of Cl-IB-MECA is surrounded by hydrophobic residues, $V169^{EL2}$ and $I253^{6.58}$, as shown in Figures 6B and 7D. The N^6-bulky group extends an additional interaction between EL2 and upper TMH6, making stronger interactions at hAA_3R.

To understand the origin of subtype selectivity, we matched the predicted best binding pose of the highly A_3-selective ligand Cl-IB-MECA to the $hAA_{2A}R$ predicted structure, and then we used SCREAM[28] to predict the optimum side chain position of residues in the binding pocket, after which we minimized the final ligand/protein

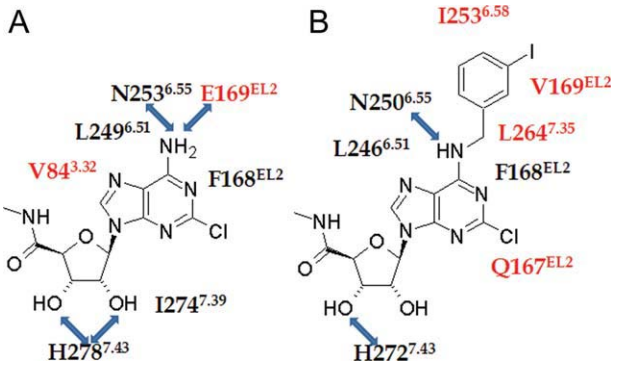

Figure 6
Schematic of the predicted binding sites for adenosine receptor agonists based on the cavity binding energies. Left: adenosine at $hAA_{2A}R$; Right: Cl-IB-MECA at hAA_3R. [Color figure can be viewed in the online issue, which is available at wileyonlinelibrary.com.]

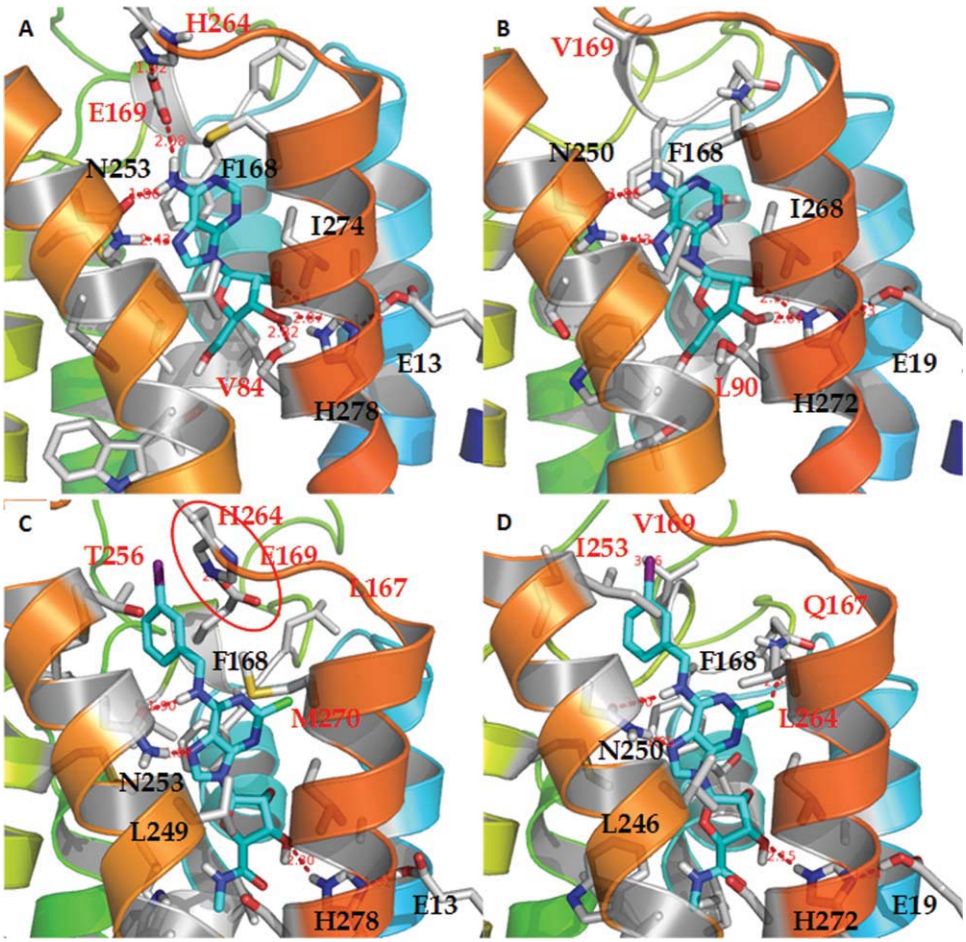

Figure 7

Predicted binding sites (**A**) adenosine to the adenosine A_{2A} receptor ($AA_{2A}R$), (**B**) adenosine to the adenosine A_3 receptor (AA_3R), (**C**) A_3 selective agonist Cl-IB-MECA at $AA_{2A}R$, (**D**) A_3 selective agonist Cl-IB-MECA at AA_3Rs. The high selectivity of Cl-IB-MECA for AA_3R relative to $AA_{2A}R$ is due to the salt-bridge between E169 and H264 [red circle in (C)] in AA_3R. In $AA_{2A}R$ we have V169 but there is no residue corresponding to H264 because of the gap in $AA_{2A}R$. H-bonding is indicated by red dots, and subtype selective residues are shown in red.

complex post neutralization. In $hAA_{2A}R$, the residue-ligand interactions were hampered by the constrained loop between $E169^{EL2}$ and $H264^{EL3}$ via a salt-bridge, as shown in Figure 7C. The corresponding amino acids of $I253^{6.58}$, $V169^{EL2}$, and $Q167^{EL2}$ in hAA_3R are $T256^{6.58}$, $E169^{EL2}$, and $L167^{EL2}$ in $hAA_{2A}R$. All three subtype variable residues in $hAA_{2A}R$ show weakened interactions in the cavity of $hAA_{2A}R$ in Table 5, resulting in a 7.31 kcal/mol favorable interaction in hAA_3R. This predicted structure is consistent with the experimental binding affinity of A_3 subtype selective Cl-IB-MECA (AA_3R Ki: 1.4 nM vs. $AA_{2A}R$ Ki, 5,360 nM).[47] The docking result also agrees with experimental observations, where the subtype selectivity of adenosine derivatives as AR agonists has been probed extensively, principally through modification of the N^6-amine moiety (where large hydrophobic groups tend to produce AA_1R and AA_3R selectivity) and the C2 position (where large hydrophobic groups tend to produce $AA_{2A}R$ selectivity).[48]

Based on the docking studies of the subtype selective antagonists, we suggest that $I253^{6.58}$ and $V169^{EL2}$ in hAA_3R are involved in vdw interactions with the N^6-bulky group in the A_3 selective ligands, while $E169^{EL2}$ in $hAA_{2A}R$ (which is the corresponding amino acid of $V169^{EL2}$ in hAA_3R) interacts with the free amino group of the A_{2A} selective ligands through additional H-bonding. Thus this predicted structure explains the increase of A_3 selectivity for the additional N^6-bulky substituent at hAA_3R. However, $Q167^{EL2}$ in hAA_3R is located in the proximity of the C2 substituent which is oriented toward the EC2 in the docking model. The corresponding amino acid $L167^{EL2}$ in $hAA_{2A}R$ might explain the increase of A_{2A} selectivity for large hydrophobic C2 substituents which are found in most A_{2A} selective antagonists.[48]

Table V
Cavity Energy of the A_3 Selective Cl-IB-MECA Bound to the Human Adenosine A_3 (AA_3R) and A_{2A} Receptors ($AA_{2A}R$)

AA_3R Ki: 1.4 nM						$AA_{2A}R$ Ki: 5360 nM					
Res	#	VdW	Coulomb	H-Bond	NonBond	Res	#	VdW	Coulomb	H-Bond	NonBond
PHE	168	−9.22	−0.56	0.00	−9.79	PHE	168	−7.54	−0.46	0.00	−7.99
ASN	250	2.46	−1.15	−5.74	−4.44	ASN	253	6.32	−1.64	−10.54	−5.86
LEU	246	−4.49	0.22	0.00	−4.28	LEU	249	−4.42	0.23	0.00	−4.19
HSE	272	−1.15	−0.57	−1.64	−3.35	HSE	278	−1.44	−0.24	−0.88	−2.55
LEU	**264**	**−2.77**	**−0.10**	**0.00**	**−2.87**	**MET**	**270**	**−3.50**	**−0.01**	**0.00**	**−3.49**
ILE	**253**	**−2.71**	**−0.16**	**0.00**	**−2.87**	**THR**	**256**	**−0.92**	**−0.37**	**0.00**	**−1.29**
VAL	**169**	**−2.45**	**−0.37**	**0.00**	**−2.82**	**GLU**	**169**	**−1.04**	**−0.89**	**−0.01**	**−1.93**
TRP	243	−2.02	0.00	0.00	−2.02	TRP	246	−0.98	−0.22	0.00	−1.20
ILE	268	−1.87	−0.04	0.00	−1.91	ILE	274	−2.99	−0.11	0.00	−3.10
MET	177	−1.63	−0.09	0.00	−1.72	MET	177	−1.62	−0.11	0.00	−1.73
GLN	**167**	**−0.64**	**−0.57**	**−0.17**	**−1.38**	**LEU**	**167**	**0.00**	**0.00**	**0.00**	**0.00**
THR	**87**	**−0.86**	**−0.51**	**0.00**	**−1.37**	**ALA**	**81**	**−0.35**	**−0.39**	**0.00**	**−0.75**
LEU	**90**	**−1.25**	**−0.03**	**0.00**	**−1.28**	**VAL**	**84**	**−1.67**	**−0.07**	**0.00**	**−1.74**
SER	271	−0.84	−0.21	0.00	−1.05	SER	277	0.20	−0.03	0.00	0.17
MET	174	−1.09	0.04	0.00	−1.05	MET	174	0.34	0.38	0.00	0.72
TYR	265	−0.59	−0.08	0.00	−0.67	TYR	271	−0.48	−0.14	0.00	−0.63
MET	**172**	**−0.63**	**−0.02**	**0.00**	**−0.65**	**VAL**	**172**	**−0.61**	**−0.06**	**0.00**	**−−0.66**
THR	94	−0.39	−0.22	0.00	−0.61	THR	88	−0.06	0.06	0.00	0.01
ILE	249	−0.57	0.03	0.00	−0.53	ILE	252	−0.61	0.04	0.00	−0.57
LEU	91	−0.50	0.02	0.00	−0.48	LEU	85	−0.93	0.01	0.00	−0.92
VAL	**72**	**−0.33**	**−0.07**	**0.00**	**−0.40**	**ILE**	**66**	**−0.47**	**0.05**	**0.00**	**−0.42**
ALA	69	−0.37	0.00	0.00	−0.38	ALA	63	−0.57	−0.05	0.00	−0.62
VAL	**65**	**−0.35**	**0.11**	**0.00**	**−0.25**	**ALA**	**59**	**−0.16**	**0.17**	**0.00**	**0.01**
SER	**242**	**−0.13**	**0.07**	**0.00**	**−0.05**	**CYS**	**245**	**−0.10**	**−0.05**	**0.00**	**−0.15**
ARN	**173**	**0.00**	**0.00**	**0.00**	**0.00**	**PRO**	**173**	**−0.26**	**0.02**	**0.00**	**−0.24**
GLY	**257**	**0.00**	**0.00**	**0.00**	**0.00**	**PRO**	**260**	**−0.36**	**−0.03**	**0.00**	**−−0.40**
						HIS	**264**	**0.95**	**−0.31**	**0.00**	**0.64**
SUM					**−46.17**	**SUM**					**−−38.86**

The residues are ordered by the total NonBond energy (A_3), which is the sum of van der Waals (vdW), Coulomb, and H-bond energy (kcal/mol) in the unified cavity. Subtype residues that vary between A_{2A} and A_3 are displayed in bold face. The main interactions leading to subtype selectivity (underlined) are I253 in A_3 vs. T256 in A_{2A}, V169 in A_3 vs E169 in A_{2A}, and Q167 in A_3 vs L167 in A_{2A}, leading to 3.85 of the predicted 7.31 differential binding. The other major differences, involving conserved residues are for F168, S273, M174 favoring A_3 and N250, I268 favoring A_{2A}, leading to a differential of 2.16 of the predicted 7.31 differential binding. The color coding for contributions of each residue to binding of the adenosine ligand is: Dark gray: > 3 kcal/mol, Gray: 1–3 kcal/mol, Light gray: 0.5–1.0 kcal/mol.

CONCLUSIONS

We used the GEnSeMBLE Monte Carlo Technique to predict an ensemble of the 20 top apo-protein predicted structures for all four subtypes of the human adenosine receptor. For hAA_3R we used the DarwinDock Monte Carlo Technique to predict the best binding pose for four subtype selective agonists and antagonists.

We find that all four selective agonists prefer what was the 15th predicted structure of the apo protein. In addition, all four change the W6.48 conformational state from *gauche+* (vertical) to *trans* (horizontal). This is consistent with observations in other GPCRs that switching of W6.48 from *gauche+* (vertical) to *trans* (horizontal) is associated with activation of the G-Protein.

In contrast the four selective antagonists all prefer ether the 2nd or 3rd conformation of the apo protein. However the situation with respect to the toggle switch is mixed. MRS5127 and LJ1251, for which the ribose is dramatically modified, retain the *gauche+* conformational of W6.48 found in the apo protein for all 20 low lying conformations. However MRS1292 and MRS3771, which retain the ribose unit of the adenosine agonist but with substitutions for the CH_2OH, prefer the trans (active) conformation in the lowest *E* conformation, but has the *gauche+* conformation for various low lying cases.

These results provide strong support for the role of W6.48 as a rotamer toggle switch affecting activation, suggesting that our methods have successfully found the ensemble of low lying conformations relevant for ligand binding and for activation of the GPCR.

We also predicted the low lying conformations of the adenosine A_{2B}, A_1, and A_3 receptors subtypes finding:

1. Excellent agreement of subtype specificities for binding of the A_3 selective Cl-IB-MECA and A_{2A} selective adenosine agonists between these two ARs.
2. Excellent agreement between the binding site of the adenosine agonist bound to $hAA_{2A}R$ with available mutation data.

These results suggest that these computational methods can predict the ensemble of low lying predicted structures accurately enough to extract information

relevant for understanding activation and accurately enough to predict the changes in conformation for different subtypes. Moreover the detailed binding sites are accurate enough to predict the differential binding characteristics between different subtypes and between agonists and antagonists binding to the same subtype. This suggests that these methods may be useful for designing subtype selective ligands for GPCR targets, even when no experimental structural information is available.

The success of these studies relies in part on having an experimental structure of $hAA_{2A}R$, indicating the value of having a crystal structure of a related system. The theory can then build on this structure to predict the structures of other subtypes. Moreover the theory can then predict the structures for agonists not yet available from experiment.

ACKNOWLEDGMENTS

Lindsay Riley participated in 2009 program of Southern California Bioinformatics Summer Institute (SoCalBSI). The authors thank Dr. Jenelle Bray and Dr. Ravi Abrol for sharing their SuperBiHelix and BiHelix protocols before publication.

REFERENCES

1. Jacobson KA, Gao ZG. Adenosine receptors as therapeutic targets. Nat Rev Drug Discov 2006;5:247–264.
2. Jacobson KA, Costanzi S, Kim S-K, Rho E, Joshi BV, Tchilibon S, Duong HT, Gao Z-G. Nucleosides, Action of nucleosides and nucleotides at 7 transmembrane-spanning receptors. Nucleosides Nucleotides Nucleic Acids 2006;25:1425–1436.
3. Vu CB, Shields P, Peng B, Kumaravel G, Jin X, Phadke D, Wang J, Engber T, Ayyub E, Petter RC. Triamino derivatives of triazolotriazine and triazolopyrimidine as adenosine A2A receptor antagonists. Bioorg Med Chem Lett 2004;14:4835–4838.
4. Tracey WR, Magee WP, Oleynek JJ, Hill RJ, Smith AH, Flynn DM, Knight DR. Novel N6-substituted adenosine 5-*N*-methyluronamides with high selectivity for human adenosine A3 receptors reduce ischemic myocardial injury. Am J Physiol Heart Circ Physiol 2003;285:H2780–H2787.
5. Shneyvais V, Mamedova L, Zinman T, Jacobson KA, Shainberg A. Activation of A3 adenosine receptor protects against doxorubicin-induced cardiotoxicity. J Mol Cell Cardiol 2001;33:1249–1261.
6. Yang H, Avila MY, Peterson-Yantorno K, Coca-Prados M, Stone RA, Jacobson KA, Civan MM. The cross-species A3 adenosine-receptor antagonist MRS1292 inhibits adenosine-triggered human nonpigmented ciliary epithelial cell fluid release and reduces mouse intraocular pressure. Current Eye Res 2005;30:747–754.
7. Goddard III WA, Kim SK, Li Y, Trzaskowski B, Griffith AR, Abrol R. Predicted 3D structures for adenosine receptors bound to ligands: comparison to the crystal structure. J Struct Biol 2010;170:10–20.
8. Warne T, Serrano-Vega MJ, Baker JG, Moukhametzianov R, Edwards PC, Henderson R, Leslie AGW, Tate CG, Schertler GFX. Structure of a β1-adrenergic G-protein coupled receptor. Nature 2008;454:486–491.
9. Jaakola VP, Griffith MT, Hanson MA, Cherezov V, Chien EY, Lane JR, Ijzerman AP, Stevens RC. The 2.6 angstrom crystal structure of a human A2A adenosine receptor bound to an antagonist. Sci 2008;322:1211–1277.
10. Cherezov V, Rosenbaum DM, Hanson MA, Rasmussen SGF, Thian FS, Kobilka TS, Choi H-J, Kuhn P, Weis WI, Kobilka BK, Stevens RC. High-resolution crystal structure of an engineered human beta2-adrenergic G protein-coupled receptor. Sci 2007;318:1258–1265.
11. Vaidehi N, Floriano WB, Trabanino R, Hall SE, Freddolino P, Choi EJ, Goddard WA, III. Structure and function of GPCRs. Proc Natl Acad Sci USA 2002;99:12622–12627.
12. Floriano WB, Vaidehi N, Zamanakos G, Goddard IIIWA. HierVLS hierarchical docking protocol for virtual ligand screening of large-molecule databases. J Med Chem 2004;47:56–71.
13. Cho AE, Wendel JA, Vaidehi N, Kekenes-Huskey PM, Floriano WB, Maiti PK, Goddard WA, III The MPSim-dock hierarchical docking algorithm: application to the eight trypsin inhibitor co-crystals. J Comp Chem 2005;26:48–71.
14. Kalani Y, Vaidehi N, Hall SE, Floriano WB, Trabanino RJ, Freddolino PL, Kam V, Goddard WA, III. Three-dimensional structure of the human D2 dopamine receptor and the binding site and binding affinities for agonists and antagonists. Proc Natl Acad Sci USA 2004;101:3815–3820.
15. Freddolino PL, Kalani MY, Vaidehi N, Floriano WB, Trabanino RJ, Freddolino PL, Kam V, Goddard WA, III. Structure and function prediction for human b2- adrenergic receptor. Proc Natl Acad Sci USA 2004;101:2736–2741.
16. Spijker P, Vaidehi N, Freddolino PL, Hilbers PA, Goddard WA, III. Dynamic behavior of fully solvated b2-adrenergic receptor, embedded in the membrane with bound agonist or antagonist. Proc Natl Acad Sci USA 2006;103:4882–4887.
17. Peng JY, Vaidehi N, Hall SE, Goddard WA, III. The predicted 3D structures of the human M1 muscarinic acetylcholine receptor with agonist or antagonist bound. Chem Med Chem 2006;1:878–890.
18. Vaidehi N, Schlyer S, Trabanino RJ, Floriano WB, Abrol R, Sharma S, Kochanny M, Koovakat S, Dunning L, Liang M, Fox JM, de Mendonca FL, Pease JE, Goddard WA, III, Horuk R. Predictions of CCR1 chemokine receptor structure and BX 471 antagonist binding followed by experimental validation. J Biol Chem 2006;281:27613–27620.
19. Heo J, Han S-K, Vaidehi N, Wendel J, Kekenes-Huskey P, Goddard WA, III. Prediction of the 3D structure of FMRF-amide neutopeptides bound to the mouse MrgC11 GPCR and experimental validation. Chem Bio Chem 2007;8:1527–1539.
20. Heo J, Vaidehi N, Wendel J, Goddard WA, III. Prediction of the 3-D structure of rat MrgA G protein-coupled receptor and identification of its binding site. J Mol Graph Model 2007;26:800–812.
21. Li Y, Zhu F, Vaidehi N, Goddard III WA, Sheinerman F, Reiling S, Morize I, Mu L, Harris K, Ardati A, Laoui A. Prediction of the 3D structure and dynamics of human DP G-protein coupled receptor bound to an agonist and an antagonist. J Am Chem Soc 2007;129:10720–10731.
22. Bray JK, Goddard WA, III. The structure of human serotonin 2c G-protein-coupled receptor bound to agonists and antagonists. J Mol Graph Model 2008;27:66–81.
23. Katoh K, Kuma K, Toh H, Miyata T. MAFFT version 5: improvement in accuracy of multiple sequence alignment. Nucleic Acid Res 2005;33:511–518.
24. Wimley WC, Creamer TP, White SH. Solvation energies of amino acid side chains and backbone in a family of host-guest pentapeptides. Biochem 1996;35:5109–5124.
25. Hessa T M-BN, Bernsel A, Kim H, Sato Y, Lerch-Bader M, Nilsson I, White SH, von Heijne G. Molecular code for transmembrane-helix recognition by the Sec61 translocon. Nature 2007;450:1026–1030.
26. Raghava GPS. APSSP2: a combination method for protein secondary structure prediction based on neural network and example based learning. CASP5 2002:A-132.
27. Pollastri G, McLysaght A. Porter: a new, accurate server for protein secondary structure prediction. Bioinformatics 2005;21:1719–1720.

28. Kam VWT, Goddard WA, III. Flat-bottom strategy for improved accuracy in protein side-chain placements. J Chem Theo Comp 2008;4:2160–2169.
29. Okada T, Sugihara M, Bondar AN, Elstner M, Entel P, Buss V. The retinal conformation and its environment in rhodopsin in light of a new 2.2 Å crystal structure. J Mol Biol 2004;342:571–583.
30. Park JH, Scheerer P, Hofmann KP, Choe HW, Ernst OP. Crystal structure of the ligand-free G-protein-coupled receptor opsin. Nature 2008;454:183–187.
31. Mayo SL, Olafson BD, Goddard III WA. DREIDING—a generic force field for molecular simulations. J Phys Chem 1990;94:8897–8909.
32. Kim S-K, Li Y, Park C, Abrol R, Goddard WA, III. Prediction of the 3D structure for the rat urotensin II receptor and comparison of the antagonist binding sites and binding selectivity between human and rat from atomistic simulations. Chem Med Chem 2010;5:1594–1608.
33. Bhandarkar M, Brunner R, Chipot C, Dalke A, Dixit S, Grayson P, Gullingsrud J, Gursoy A, Hardy D, Hénin J, Humphrey W, Hurwitz D, Krawetz N, Kumar S, Nelson M, Phillips J, Schinozaki A, Zheng G, Zhu F.NAMD User's Guide. Theoretical Biophysics Group, University of Illinois at Urbana-Champaign and Beckman Institute, Urbana, 2008; Version 2.6.
34. Phillips JC, Braun R, Wang W, Gumbart J, Tajkhorshid E, Villa E, Chipot C, Skeel RD, Kale L, K. S. Scalable molecular dynamics with NAMD. J Comput Chem 2005;26:1781–1802.
35. MacKerell AD, Bashford D, Bellott M, Dunbrack RL, Evanseck JD, Field MJ, Fischer S, Gao J, Guo H, Ha S, Joseph-McCarthy D, Kuchnir L, Kuczera K, Lau FTK, Mattos C, Michnick S, Ngo T, Nguyen DT, Prodhom B, Reiher WE, Roux B, Schlenkrich M, Smith JC, Stote R, Straub J, Watanabe M, Wiorkiewicz-Kuczera J, Yin D, Karplus M. All-atom empirical potential for molecular modeling and dynamics studies of proteins. J Phys Chem B 1998;102:3586–3616.
36. Feller SE, Yin D, Pastor RW, MacKerell AD Jr. Molecular dynamics simulation of unsaturated lipids at low hydration: parametrization and comparison with diffraction studies. Biophys J 1997;73:2269–2279.
37. Melman A, Wang B, Joshi BV, Gao ZG, Castro S, Heller CL, Kim S-K, Jeong LS, Jacobson KA. Selective A(3) adenosine receptor antagonists derived from nucleosides containing a bicyclo[3.1.0]hexane ring system. Bioorg Med Chem 2008;16:8546–8556.
38. Tosh DK, Chinn M, Ivanov AA, Klutz AM, Gao ZG, Jacobson KA. Functionalized congeners of A3 adenosine receptor-selective nucleosides containing a bicyclo[3.1.0]hexane ring system. J Med Chem 2009;52:7580–7592.
39. Ruprecht JJ, Mielke T, Vogel R, Villa C, Schertler GFX. Electron crystallography reveals the sturcture of metarhodopsin I. EMBO J 2004;23:3609–3620.
40. Pellissier LP, Sallander J, Campillo M, Gaven F, Queffeulou E, Pillot M, Dumuis A, Claeysen S, Bockaert J, Pardo L. Conformational toggle switches implicated in basal constitutive and agonist-induced activated states of 5-hydroxytryptamine-4 receptors. Mol Pharmacol 2009;75:982–990.
41. Nygaard ,R, Frimurer TM, Holst B, Rosenkilde MM, Schwartz TW. Ligand binding and micro-switches in 7TM receptor structures. Trends Pharmacol Sci 2009;30:249–259.
42. Gao Z-G, Chen A, Barak D, Kim S-K, Muller CE, Jacobson KA. Identification by site-directed mutagenesis of residues involved in ligand recognition and activation of the human A3 adenosine receptor. J Biol Chem 2002;277:19056–19063.
43. Kim S-K, Gao Z-G, Jeong LS, Jacobson KA. Docking studies of agonists and antagonists suggest an activation pathway of the A3 adenosine receptor. J Mol Graph Model 2006;25:562–577.
44. Shi L, Liapakis G, Xu R, Guarnieri F, Ballesteros JA, Javitch JA. Beta2 adrenergic receptor activation. Modulation of the proline kink in transmembrane 6 by a rotamer toggle switch. J Biol Chem 2002;277:40989–40996.
45. Jacobson KA, Ji X, Li AH, Melman N, Siddiqui MA, Shin KJ, Marquez VE, Ravi RG. Methanocarba analogues of purine nucleosides as potent and selective adenosine receptor agonists. J Med Chem 2000;43:2196–2203.
46. Kim S-K, Gao Z-G, Van Rompaey P, Gross AS, Chen A, Van Calenbergh S, Jacobson KA. Modeling the adenosine receptors: comparison of the binding domains of A2A agonists and antagonists. J Med Chem 2003;46:4847–4859.
47. Jeong LS, Choe SA, Gunaga P, Kim HO, Lee HW, Lee SK, Tosh DK, Patel A, Palaniappan KK, Gao ZG, Jacobson KA, Moon HR. Discovery of a new nucleoside template for human A3 adenosine receptor ligands: D-4′-thioadenosine derivatives without 4′-hydroxymethyl group as highly potent and selective antagonists. J Med Chem 2007;50:3159–3162.
48. Jacobson KA, Klutz AM, Tosh DK, Ivanov AA, Preti D, Baraldi PG. Medicinal chemistry of the A3 adenosine receptor: agonists, antagonists, and receptor engineering. Handbook Exp Pharmacol 2009;193:123–159.